

High-quality two-nucleon potentials up to fifth order of the chiral expansion

D. R. Entem,^{1,*} R. Machleidt,^{2,†} and Y. Nosyk²

¹*Grupo de Física Nuclear, IUFFyM, Universidad de Salamanca, E-37008 Salamanca, Spain*

²*Department of Physics, University of Idaho, Moscow, Idaho 83844, USA*

(Dated: February 27, 2022)

We present NN potentials through five orders of chiral effective field theory ranging from leading order (LO) to next-to-next-to-next-to-next-to-leading order (N⁴LO). The construction may be perceived as consistent in the sense that the same power counting scheme as well as the same cutoff procedures are applied in all orders. Moreover, the long-range parts of these potentials are fixed by the very accurate πN LECs as determined in the Roy-Steiner equations analysis by Hoferichter, Ruiz de Elvira and coworkers. In fact, the uncertainties of these LECs are so small that a variation within the errors leads to effects that are essentially negligible, reducing the error budget of predictions considerably. The NN potentials are fit to the world NN data below pion-production threshold of the year of 2016. The potential of the highest order (N⁴LO) reproduces the world NN data with the outstanding χ^2/datum of 1.15, which is the highest precision ever accomplished for any chiral NN potential to date. The NN potentials presented may serve as a solid basis for systematic *ab initio* calculations of nuclear structure and reactions that allow for a comprehensive error analysis. In particular, the consistent order by order development of the potentials will make possible a reliable determination of the truncation error at each order. Our family of potentials is non-local and, generally, of soft character. This feature is reflected in the fact that the predictions for the triton binding energy (from two-body forces only) converges to about 8.1 MeV at the highest orders. This leaves room for three-nucleon-force contributions of moderate size.

PACS numbers: 13.75.Cs, 21.30.-x, 12.39.Fe

Keywords: nucleon-nucleon scattering, chiral perturbation theory, chiral effective field theory

I. INTRODUCTION

The quest for a practically feasible, and yet fundamental, theory of hadronic interactions at low energy (where QCD is non-perturbative) has spanned several decades. At the present time, there exists a general consensus that chiral effective field theory (chiral EFT) may provide the best answer to the quest. By its nature, chiral EFT is a model-independent approach with firm roots in QCD, due to the fact that interactions are subjected to the constraints of the broken chiral symmetry of low-energy QCD. Moreover, the approach is systematic in the sense that the various contributions to a particular dynamical process can be arranged as an expansion in terms of a suitable “parameter”. The latter is chosen to be the ratio of a typical external momentum (soft scale) to the chiral symmetry breaking scale (≈ 1 GeV, hard scale). Recent comprehensive reviews on the subject can be found in Refs. [1, 2].

In its early stages, chiral perturbation theory (ChPT) was applied mostly to $\pi\pi$ [3] and πN [4] dynamics, because, due to the Goldstone-boson nature of the pion, these are the most natural scenarios for a perturbative expansion to exist. In the meantime, though, chiral EFT has been applied in nucleonic systems by numerous groups [1, 2, 5–30]. Derivations of the nucleon-nucleon (NN) interaction up to fourth order (next-to-next-to-next-to-leading order, N³LO) can be found in Refs. [7, 9, 10, 12, 13, 15], with quantitative NN potentials making their appearance in the early 2000’s [16, 17].

Since then, a wealth of applications of N³LO NN potentials together with chiral three-nucleon forces (3NFs) have been reported. These investigations include few-nucleon reactions [31–34], structure of light- and medium-mass nuclei [35–38], and infinite matter [39–44]. Although satisfactory predictions have been obtained in many cases, persistent problems continue to pose serious challenges, such as the well-known ‘ A_y puzzle’ of nucleon-deuteron scattering [45]. Naturally, one would invoke 3NFs as the most likely mechanism to solve this problem. Unfortunately, the chiral 3NF at NNLO does only very little to improve the situation with nucleon-deuteron scattering [31, 33], while inclusion of the N³LO 3NF produces an effect in the wrong direction [34]. The next step is then to proceed systematically in the expansion, namely to look at N⁴LO (or fifth order). This order is interesting for diverse reasons. From studies of some of the 3NF topologies at N⁴LO [46, 47], we know that a complete set of isospin-spin-momentum

*Electronic address: entem@usal.es

†Electronic address: machleidt@uidaho.edu

3NF structures (a total of 20) are present at this order [48] and that contributions can be of substantial size. Even more promising, at this order a new set of 3NF contact interactions appears, which has recently been derived by the Pisa group [49]. Contact terms are relatively easy to work with and, most importantly, come with free coefficients and, thus, provide larger flexibility and a great likelihood to solve persistent problems such as the A_y puzzle as well as other issues (like, the “radius problem” [50] and the overbinding of intermediate-mass nuclei [51]).

A principle of all EFTs is that, for meaningful predictions, it is necessary to include *all* contributions that appear at the order at which the calculation is conducted. Thus, when nuclear structure problems require for their solution the inclusion of 3NFs at N⁴LO, then also the two-nucleon force involved in the calculation has to be of order N⁴LO. This is one reason why in Ref. [52] we derived the N⁴LO two-pion exchange (2PE) and three-pion exchange (3PE) contributions to the NN interaction and tested them in peripheral partial waves. In this paper, we will present complete N⁴LO NN potentials that also include the lower partial waves which receive contributions from contact interactions.

In Ref. [52], we also demonstrated that the next-to-next-to-leading order (NNLO), the N³LO, and the N⁴LO contributions to the NN interaction are all of about the same size, thus, not showing much of a trend towards convergence. Therefore, in Ref. [53] we calculated the N⁵LO (sixth order) contribution which, indeed, turned out to be small. The latter result may be perceived as an indication of convergence showing up at N⁵LO. This adds to the significance of order N⁴LO.

Besides the above, we are faced with another set of convergence issues: The convergence of the predictions for the properties of nuclear few- and many-body systems, in which also chiral many-body forces are involved. To investigate these issues, one needs (besides those many-body forces) NN potentials at all orders of chiral EFT, ranging from leading order (LO) to N⁴LO, and constructed consistently, i. e., using the same power-counting scheme, consistent LECs, etc..

For that reason, we present in this paper NN potentials through five orders from LO to N⁴LO, constructed with the above-stated consistencies and with a reproduction of the NN data of the maximum quality possible at the respective orders. These potentials will allow for systematic investigations of nuclear few- and many-body systems with clear implications for convergence and uncertainty quantifications (truncation errors) [23, 27, 54, 55].

This paper is organized as follows: In Sec. II, we present the expansion of the NN potential through all orders from LO to N⁴LO. The reproduction of the NN scattering data and the deuteron properties are given in Sec. III. Some aspects regarding 3NFs are discussed in Sec. IV, and uncertainty quantification is considered in Sec. V. Sec. VI concludes the paper.

II. EXPANSION OF THE NN POTENTIAL

A. Effective Lagrangians

In the Δ -less version of chiral EFT, which is the one we are pursuing here, the relevant degrees of freedom are pions (Goldstone bosons) and nucleons. Since the interactions of Goldstone bosons must vanish at zero momentum transfer and in the chiral limit ($m_\pi \rightarrow 0$), the low-energy expansion of the effective Lagrangian is arranged in powers of derivatives and pion masses. This effective Lagrangian is subdivided into the following pieces,

$$\mathcal{L}_{\text{eff}} = \mathcal{L}_{\pi\pi} + \mathcal{L}_{\pi N} + \mathcal{L}_{NN} + \dots, \quad (2.1)$$

where $\mathcal{L}_{\pi\pi}$ deals with the dynamics among pions, $\mathcal{L}_{\pi N}$ describes the interaction between pions and a nucleon, and \mathcal{L}_{NN} contains two-nucleon contact interactions which consist of four nucleon-fields (four nucleon legs) and no meson fields. The ellipsis stands for terms that involve two nucleons plus pions and three or more nucleons with or without pions, relevant for nuclear many-body forces. The individual Lagrangians are organized in terms of increasing orders:

$$\mathcal{L}_{\pi\pi} = \mathcal{L}_{\pi\pi}^{(2)} + \mathcal{L}_{\pi\pi}^{(4)} + \dots, \quad (2.2)$$

$$\mathcal{L}_{\pi N} = \mathcal{L}_{\pi N}^{(1)} + \mathcal{L}_{\pi N}^{(2)} + \mathcal{L}_{\pi N}^{(3)} + \mathcal{L}_{\pi N}^{(4)} + \dots, \quad (2.3)$$

$$\mathcal{L}_{NN} = \mathcal{L}_{NN}^{(0)} + \mathcal{L}_{NN}^{(2)} + \mathcal{L}_{NN}^{(4)} + \dots, \quad (2.4)$$

where the superscript refers to the number of derivatives or pion mass insertions (chiral dimension) and the ellipses stand for terms of higher dimensions. We use the heavy-baryon formulation of the Lagrangians, the explicit expressions of which can be found in Refs. [1, 46].

B. Power counting

Based upon the above Lagrangians, an infinite number of diagrams contributing to the interactions among nucleons can be drawn. Nuclear potentials are defined by the irreducible types of these graphs. By definition, an irreducible graph is a diagram that cannot be separated into two by cutting only nucleon lines. These graphs are then analyzed in terms of powers of small external momenta over the large scale: $(Q/\Lambda_\chi)^\nu$, where Q is generic for a momentum (nucleon three-momentum or pion four-momentum) or a pion mass and $\Lambda_\chi \sim 1$ GeV is the chiral symmetry breaking scale (hadronic scale, hard scale). Determining the power ν has become known as power counting.

Following the Feynman rules of covariant perturbation theory, a nucleon propagator is Q^{-1} , a pion propagator Q^{-2} , each derivative in any interaction is Q , and each four-momentum integration Q^4 . This is also known as naive dimensional analysis or Weinberg counting.

Since we use the heavy-baryon formalism, we encounter terms which include factors of Q/M_N , where M_N denotes the nucleon mass. We count the order of such terms by the rule $Q/M_N \sim (Q/\Lambda_\chi)^2$, for reasons explained in Ref. [5].

Applying some topological identities, one obtains for the power of a connected irreducible diagram involving A nucleons [1, 5]

$$\nu = -2 + 2A - 2C + 2L + \sum_i \Delta_i, \quad (2.5)$$

with

$$\Delta_i \equiv d_i + \frac{n_i}{2} - 2, \quad (2.6)$$

where L denotes the number of loops in the diagram; d_i is the number of derivatives or pion-mass insertions and n_i the number of nucleon fields (nucleon legs) involved in vertex i ; the sum runs over all vertexes i contained in the connected diagram under consideration. Note that $\Delta_i \geq 0$ for all interactions allowed by chiral symmetry.

An important observation from power counting is that the powers are bounded from below and, specifically, $\nu \geq 0$. This fact is crucial for the convergence of the low-momentum expansion.

Furthermore, the power formula Eq. (2.5) allows to predict the leading orders of connected multi-nucleon forces. Consider a m -nucleon irreducibly connected diagram (m -nucleon force) in an A -nucleon system ($m \leq A$). The number of separately connected pieces is $C = A - m + 1$. Inserting this into Eq. (2.5) together with $L = 0$ and $\sum_i \Delta_i = 0$ yields $\nu = 2m - 4$. Thus, two-nucleon forces ($m = 2$) appear at $\nu = 0$, three-nucleon forces ($m = 3$) at $\nu = 2$ (but they happen to cancel at that order), and four-nucleon forces at $\nu = 4$ (they don't cancel).

For an irreducible NN diagram ($A = 2$, $C = 1$), the power formula collapses to the very simple expression

$$\nu = 2L + \sum_i \Delta_i. \quad (2.7)$$

In summary, the chief point of the ChPT expansion of the potential is that, at a given order ν , there exists only a finite number of graphs. This is what makes the theory calculable. The expression $(Q/\Lambda_\chi)^{\nu+1}$ provides an estimate of the relative size of the contributions left out and, thus, of the relative uncertainty at order ν . The ability to calculate observables (in principle) to any degree of accuracy gives the theory its predictive power.

Chiral perturbation theory and power counting imply that nuclear forces evolve as a hierarchy controlled by the power ν , see Fig. 1 for an overview. In what follows, we will focus on the two-nucleon force (2NF).

C. The long-range NN potential

The long-range part of the NN potential is built up from pion exchanges, which are ruled by chiral symmetry. The various pion-exchange contributions may be analyzed according to the number of pions being exchanged between the two nucleons:

$$V = V_{1\pi} + V_{2\pi} + V_{3\pi} + \dots, \quad (2.8)$$

where the meaning of the subscripts is obvious and the ellipsis represents 4π and higher pion exchanges. For each of the above terms, we have a low-momentum expansion:

$$V_{1\pi} = V_{1\pi}^{(0)} + V_{1\pi}^{(2)} + V_{1\pi}^{(3)} + V_{1\pi}^{(4)} + V_{1\pi}^{(5)} + \dots \quad (2.9)$$

$$V_{2\pi} = V_{2\pi}^{(2)} + V_{2\pi}^{(3)} + V_{2\pi}^{(4)} + V_{2\pi}^{(5)} + \dots \quad (2.10)$$

$$V_{3\pi} = V_{3\pi}^{(4)} + V_{3\pi}^{(5)} + \dots, \quad (2.11)$$

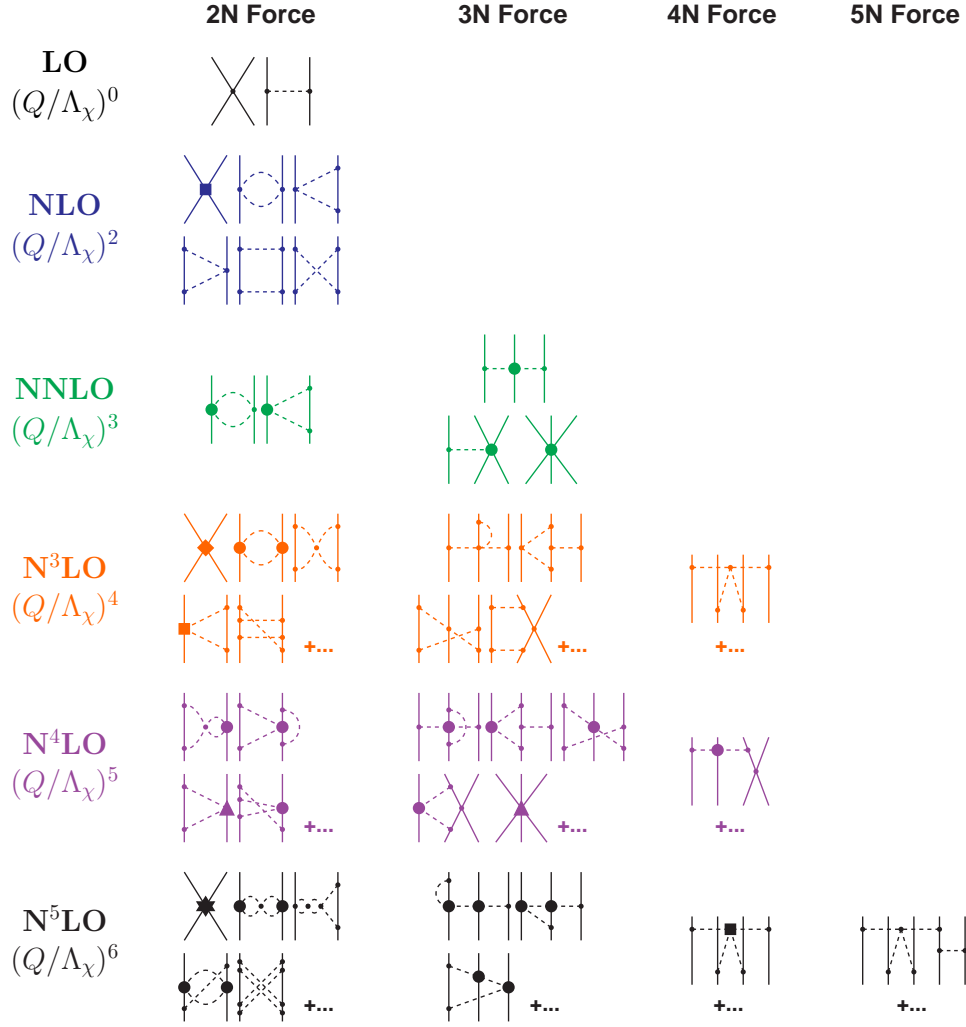


FIG. 1: Hierarchy of nuclear forces in ChPT. Solid lines represent nucleons and dashed lines pions. Small dots, large solid dots, solid squares, triangles, diamonds, and stars denote vertexes of index $\Delta_i = 0, 1, 2, 3, 4,$ and 6 , respectively. Further explanations are given in the text.

where the superscript denotes the order ν of the expansion.

Order by order, the long-range NN potential builds up as follows:

$$V_{\text{LO}} \equiv V^{(0)} = V_{1\pi}^{(0)} \quad (2.12)$$

$$V_{\text{NLO}} \equiv V^{(2)} = V_{\text{LO}} + V_{1\pi}^{(2)} + V_{2\pi}^{(2)} \quad (2.13)$$

$$V_{\text{NNLO}} \equiv V^{(3)} = V_{\text{NLO}} + V_{1\pi}^{(3)} + V_{2\pi}^{(3)} \quad (2.14)$$

$$V_{\text{N³LO}} \equiv V^{(4)} = V_{\text{NNLO}} + V_{1\pi}^{(4)} + V_{2\pi}^{(4)} + V_{3\pi}^{(4)} \quad (2.15)$$

$$V_{\text{N⁴LO}} \equiv V^{(5)} = V_{\text{N³LO}} + V_{1\pi}^{(5)} + V_{2\pi}^{(5)} + V_{3\pi}^{(5)} \quad (2.16)$$

where LO stands for leading order, NLO for next-to-leading order, etc..

TABLE I: Basic constants used throughout this work [56].

Quantity	Value
Axial-vector coupling constant g_A	1.29
Pion-decay constant f_π	92.4 MeV
Charged-pion mass m_{π^\pm}	139.5702 MeV
Neutral-pion mass m_{π^0}	134.9766 MeV
Average pion-mass \bar{m}_π	138.0390 MeV
Proton mass M_p	938.2720 MeV
Neutron mass M_n	939.5654 MeV
Average nucleon-mass \bar{M}_N	938.9183 MeV

1. Leading order

At leading order, only one-pion exchange (1PE) contributes to the long range, cf. Fig. 1. The charge-independent 1PE is given by

$$V_{1\pi}^{(\text{CI})}(\vec{p}', \vec{p}) = -\frac{g_A^2}{4f_\pi^2} \boldsymbol{\tau}_1 \cdot \boldsymbol{\tau}_2 \frac{\vec{\sigma}_1 \cdot \vec{q} \vec{\sigma}_2 \cdot \vec{q}}{q^2 + m_\pi^2}, \quad (2.17)$$

where \vec{p}' and \vec{p} denote the final and initial nucleon momenta in the center-of-mass system, respectively. Moreover, $\vec{q} = \vec{p}' - \vec{p}$ is the momentum transfer, and $\vec{\sigma}_{1,2}$ and $\boldsymbol{\tau}_{1,2}$ are the spin and isospin operators of nucleon 1 and 2, respectively. Parameters g_A , f_π , and m_π denote the axial-vector coupling constant, pion-decay constant, and the pion mass, respectively. See Table I for their values. Higher order corrections to the 1PE are taken care of by mass and coupling constant renormalizations. Note also that, on shell, there are no relativistic corrections. Thus, we apply 1PE in the form Eq. (2.17) through all orders.

For the NN potentials constructed in this paper, we take the charge-dependence of the 1PE due to pion-mass splitting into account. Thus, in proton-proton (pp) and neutron-neutron (nn) scattering, we actually use

$$V_{1\pi}^{(pp)}(\vec{p}', \vec{p}) = V_{1\pi}^{(nn)}(\vec{p}', \vec{p}) = V_{1\pi}(m_{\pi^0}), \quad (2.18)$$

and in neutron-proton (np) scattering, we apply

$$V_{1\pi}^{(np)}(\vec{p}', \vec{p}) = -V_{1\pi}(m_{\pi^0}) + (-1)^{I+1} 2V_{1\pi}(m_{\pi^\pm}), \quad (2.19)$$

where $I = 0, 1$ denotes the total isospin of the two-nucleon system and

$$V_{1\pi}(m_\pi) \equiv -\frac{g_A^2}{4f_\pi^2} \frac{\vec{\sigma}_1 \cdot \vec{q} \vec{\sigma}_2 \cdot \vec{q}}{q^2 + m_\pi^2}. \quad (2.20)$$

Formally speaking, the charge-dependence of the 1PE exchange is of order NLO [1], but we include it also at leading order to make the comparison with the (charge-dependent) phase-shift analyses meaningful.

2. Subleading pion exchanges

Two-pion exchange starts at NLO and continues through all higher orders. In Fig. 1, the corresponding diagrams are shown completely up to NNLO. Beyond that order, the number of diagrams increases so dramatically that we show only a few symbolic graphs. The situation is similar for the 3PE contributions which start at N³LO. Also the mathematical formulas are getting increasingly involved. A complete collection of all formulas concerning the 2PE and 3PE contributions through all orders from NLO to N⁴LO is given in Ref. [52]. Therefore, we will not reprint the complicated math here and refer the interested reader to the comprehensive compendium [52]. In all 2PE and 3PE contributions, we use the average pion mass, $\bar{m}_\pi = 138.039$ MeV. The charge-dependence caused by pion-mass splitting in 2PE has been found to be negligible in all partial waves with $L > 0$ [57]. The small effect in 1S_0 is absorbed into the charge-dependence of the zeroth-order contact parameter \tilde{C}_{1S_0} , see below.

TABLE II: The πN LECs as determined in the Roy-Steiner-equation analysis of πN scattering conducted in Ref. [60]. The given orders of the chiral expansion refer to the NN system. Note that the orders, at which the LECs are extracted from the πN system, are always lower by one order as compared of the NN system in which the LECs are applied. The c_i , \bar{d}_i , and \bar{e}_i are the LECs of the second, third, and fourth order πN Lagrangian [46] and are in units of GeV^{-1} , GeV^{-2} , and GeV^{-3} , respectively. The uncertainties in the last digits are given in parentheses after the values.

	NNLO	N ³ LO	N ⁴ LO
c_1	-0.74(2)	-1.07(2)	-1.10(3)
c_2	—	3.20(3)	3.57(4)
c_3	-3.61(5)	-5.32(5)	-5.54(6)
c_4	2.44(3)	3.56(3)	4.17(4)
$\bar{d}_1 + \bar{d}_2$	—	1.04(6)	6.18(8)
\bar{d}_3	—	-0.48(2)	-8.91(9)
\bar{d}_5	—	0.14(5)	0.86(5)
$\bar{d}_{14} - \bar{d}_{15}$	—	-1.90(6)	-12.18(12)
\bar{e}_{14}	—	—	1.18(4)
\bar{e}_{17}	—	—	-0.18(6)

The contributions have the following general decomposition:

$$\begin{aligned}
V(\vec{p}', \vec{p}) = & V_C + \boldsymbol{\tau}_1 \cdot \boldsymbol{\tau}_2 W_C \\
& + [V_S + \boldsymbol{\tau}_1 \cdot \boldsymbol{\tau}_2 W_S] \vec{\sigma}_1 \cdot \vec{\sigma}_2 \\
& + [V_{LS} + \boldsymbol{\tau}_1 \cdot \boldsymbol{\tau}_2 W_{LS}] \left(-i\vec{S} \cdot (\vec{q} \times \vec{k}) \right) \\
& + [V_T + \boldsymbol{\tau}_1 \cdot \boldsymbol{\tau}_2 W_T] \vec{\sigma}_1 \cdot \vec{q} \vec{\sigma}_2 \cdot \vec{q},
\end{aligned} \tag{2.21}$$

where $\vec{k} = (\vec{p}' + \vec{p})/2$ denotes the average momentum and $\vec{S} = (\vec{\sigma}_1 + \vec{\sigma}_2)/2$ is the total spin. For on-shell scattering, V_α and W_α ($\alpha = C, S, LS, T$) can be expressed as functions of $q = |\vec{q}|$.

We consider loop contributions in terms of their spectral functions, from which the momentum-space amplitudes $V_\alpha(q)$ and $W_\alpha(q)$ are obtained via the subtracted dispersion integrals:

$$\begin{aligned}
V_{C,S}(q) &= -\frac{2q^6}{\pi} \int_{nm_\pi}^{\tilde{\Lambda}} d\mu \frac{\text{Im} V_{C,S}(i\mu)}{\mu^5(\mu^2 + q^2)}, \\
V_{T,LS}(q) &= \frac{2q^4}{\pi} \int_{nm_\pi}^{\tilde{\Lambda}} d\mu \frac{\text{Im} V_{T,LS}(i\mu)}{\mu^3(\mu^2 + q^2)},
\end{aligned} \tag{2.22}$$

and similarly for $W_{C,S,T,LS}$. The thresholds are given by $n = 2$ for two-pion exchange and $n = 3$ for three-pion exchange. For $\tilde{\Lambda} \rightarrow \infty$ the above dispersion integrals yield the results of dimensional regularization, while for finite $\tilde{\Lambda} \geq nm_\pi$ we employ the method known as spectral-function regularization (SFR) [58]. The purpose of the finite scale $\tilde{\Lambda}$ is to constrain the imaginary parts to the low-momentum region where chiral effective field theory is applicable. Thus, a reasonable choice for $\tilde{\Lambda}$ is to keep it below the masses of the vector mesons $\rho(770)$ and $\omega(782)$, but above the $f_0(500)$ [also known as $\sigma(500)$] [56]. This suggests that the region 600-700 MeV is appropriate for $\tilde{\Lambda}$. Consequently, we use $\tilde{\Lambda} = 650$ MeV in all orders, except for N⁴LO where we apply 700 MeV. We use this slightly larger value for N⁴LO, because it is suggestive that higher orders may permit for an extension to higher momenta.

3. The pion-nucleon low-energy constants

Chiral symmetry establishes a link between the dynamics in the πN -system and the NN -system through common low-energy constants. Therefore, consistency requires that we use the LECs for subleading πN -couplings as determined in analysis of low-energy πN -scattering. Over the years, there have been many such determinations of questionable reliability. Fortunately, that has changed recently with the analysis by Hoferichter and Ruiz de Elvira [59] *et al.* [60], in which the Roy-Steiner (RS) equations are applied. The RS equations are a set of coupled partial-wave dispersion relations constraint by analyticity, unitarity, and crossing symmetry. In the work of Ref. [60], they are used to extract

the LECs from the subthreshold point in πN scattering instead of the physical region. This is the preferred method for LECs to be applied in chiral potentials where, e. g., a one-loop πN amplitude leads to a two-loop contribution in NN . Such diagrams are best evaluated by means of Cutkosky rules [12, 52, 53]. The πN amplitude that enters the dispersion integrals is weighted much closer to subthreshold kinematics than to the threshold point. The LECs determined in Ref. [60] carry very small uncertainties (cf. Table II) for, essentially, two reasons: first, because of the constraints built into the RS equations; second, because of the use of the high-accuracy πN scattering lengths extracted from pionic atoms. In fact, the uncertainties are so small that they are negligible for our purposes. This makes the variation of the πN LECs in NN potential construction obsolete and reduces the error budget in applications of these potentials. For the potentials constructed in this paper, the central values of Table II are applied.

D. The short-range NN potential

The short-range NN potential is described by contributions of the contact type, which are constrained by parity, time-reversal, and the usual invariances, but not by chiral symmetry. Terms that include a factor $\boldsymbol{\tau}_1 \cdot \boldsymbol{\tau}_2$ (owing to isospin invariance) can be left out due to Fierz ambiguity. Because of parity and time-reversal only even powers of momentum are allowed. Thus, the expansion of the contact potential is formally written as

$$V_{\text{ct}} = V_{\text{ct}}^{(0)} + V_{\text{ct}}^{(2)} + V_{\text{ct}}^{(4)} + V_{\text{ct}}^{(6)} + \dots, \quad (2.23)$$

where the superscript denotes the power or order.

The zeroth order (leading order, LO) contact potential is given by

$$V_{\text{ct}}^{(0)}(\vec{p}', \vec{p}) = C_S + C_T \vec{\sigma}_1 \cdot \vec{\sigma}_2 \quad (2.24)$$

and, in terms of partial waves,

$$V_{\text{ct}}^{(0)}({}^1S_0) = \tilde{C}_{1S_0} = 4\pi (C_S - 3C_T) \quad (2.25)$$

$$V_{\text{ct}}^{(0)}({}^3S_1) = \tilde{C}_{3S_1} = 4\pi (C_S + C_T). \quad (2.26)$$

To deal with the isospin breaking in the 1S_0 state, we treat \tilde{C}_{1S_0} in a charge-dependent way. Thus, we will distinguish between $\tilde{C}_{1S_0}^{\text{pp}}$, $\tilde{C}_{1S_0}^{\text{np}}$, and $\tilde{C}_{1S_0}^{\text{nn}}$.

At second order (NLO), we have

$$\begin{aligned} V_{\text{ct}}^{(2)}(\vec{p}', \vec{p}) &= C_1 q^2 + C_2 k^2 \\ &+ (C_3 q^2 + C_4 k^2) \vec{\sigma}_1 \cdot \vec{\sigma}_2 \\ &+ C_5 \left(-i \vec{S} \cdot (\vec{q} \times \vec{k}) \right) \\ &+ C_6 (\vec{\sigma}_1 \cdot \vec{q}) (\vec{\sigma}_2 \cdot \vec{q}) \\ &+ C_7 (\vec{\sigma}_1 \cdot \vec{k}) (\vec{\sigma}_2 \cdot \vec{k}), \end{aligned} \quad (2.27)$$

and partial-wave decomposition yields

$$\begin{aligned} V_{\text{ct}}^{(2)}({}^1S_0) &= C_{1S_0} (p^2 + p'^2) \\ V_{\text{ct}}^{(2)}({}^3P_0) &= C_{3P_0} pp' \\ V_{\text{ct}}^{(2)}({}^1P_1) &= C_{1P_1} pp' \\ V_{\text{ct}}^{(2)}({}^3P_1) &= C_{3P_1} pp' \\ V_{\text{ct}}^{(2)}({}^3S_1) &= C_{3S_1} (p^2 + p'^2) \\ V_{\text{ct}}^{(2)}({}^3S_1 - {}^3D_1) &= C_{3S_1 - {}^3D_1} p^2 \\ V_{\text{ct}}^{(2)}({}^3D_1 - {}^3S_1) &= C_{3S_1 - {}^3D_1} p'^2 \\ V_{\text{ct}}^{(2)}({}^3P_2) &= C_{3P_2} pp'. \end{aligned} \quad (2.28)$$

The relationship between the $C_{(2S+1)L_J}$ and the C_i can be found in Ref. [1].

The fourth order (N³LO) contacts are

$$\begin{aligned}
V_{\text{ct}}^{(4)}(\vec{p}', \vec{p}) &= D_1 q^4 + D_2 k^4 + D_3 q^2 k^2 + D_4 (\vec{q} \times \vec{k})^2 \\
&+ \left(D_5 q^4 + D_6 k^4 + D_7 q^2 k^2 + D_8 (\vec{q} \times \vec{k})^2 \right) \vec{\sigma}_1 \cdot \vec{\sigma}_2 \\
&+ (D_9 q^2 + D_{10} k^2) \left(-i \vec{S} \cdot (\vec{q} \times \vec{k}) \right) \\
&+ (D_{11} q^2 + D_{12} k^2) (\vec{\sigma}_1 \cdot \vec{q}) (\vec{\sigma}_2 \cdot \vec{q}) \\
&+ (D_{13} q^2 + D_{14} k^2) (\vec{\sigma}_1 \cdot \vec{k}) (\vec{\sigma}_2 \cdot \vec{k}) \\
&+ D_{15} \left(\vec{\sigma}_1 \cdot (\vec{q} \times \vec{k}) \vec{\sigma}_2 \cdot (\vec{q} \times \vec{k}) \right), \tag{2.29}
\end{aligned}$$

with contributions by partial waves,

$$\begin{aligned}
V_{\text{ct}}^{(4)}(1S_0) &= \widehat{D}_{1S_0} (p'^4 + p^4) + D_{1S_0} p'^2 p^2 \\
V_{\text{ct}}^{(4)}(3P_0) &= D_{3P_0} (p'^3 p + p' p^3) \\
V_{\text{ct}}^{(4)}(1P_1) &= D_{1P_1} (p'^3 p + p' p^3) \\
V_{\text{ct}}^{(4)}(3P_1) &= D_{3P_1} (p'^3 p + p' p^3) \\
V_{\text{ct}}^{(4)}(3S_1) &= \widehat{D}_{3S_1} (p'^4 + p^4) + D_{3S_1} p'^2 p^2 \\
V_{\text{ct}}^{(4)}(3D_1) &= D_{3D_1} p'^2 p^2 \\
V_{\text{ct}}^{(4)}(3S_1 - 3D_1) &= \widehat{D}_{3S_1 - 3D_1} p^4 + D_{3S_1 - 3D_1} p'^2 p^2 \\
V_{\text{ct}}^{(4)}(3D_1 - 3S_1) &= \widehat{D}_{3S_1 - 3D_1} p'^4 + D_{3S_1 - 3D_1} p'^2 p^2 \\
V_{\text{ct}}^{(4)}(1D_2) &= D_{1D_2} p'^2 p^2 \\
V_{\text{ct}}^{(4)}(3D_2) &= D_{3D_2} p'^2 p^2 \\
V_{\text{ct}}^{(4)}(3P_2) &= D_{3P_2} (p'^3 p + p' p^3) \\
V_{\text{ct}}^{(4)}(3P_2 - 3F_2) &= D_{3P_2 - 3F_2} p'^3 p^3 \\
V_{\text{ct}}^{(4)}(3F_2 - 3P_2) &= D_{3P_2 - 3F_2} p'^3 p^3 \\
V_{\text{ct}}^{(4)}(3D_3) &= D_{3D_3} p'^2 p^2. \tag{2.30}
\end{aligned}$$

Reference [1] provides formulas that relate the $D_{(2S+1)L_J}$ to the D_i .

The next higher order is sixth order (N⁵LO) at which, finally, also F -waves are affected in the following way:

$$\begin{aligned}
V_{\text{ct}}^{(6)}(3F_2) &= E_{3F_2} p'^3 p^3 \\
V_{\text{ct}}^{(6)}(1F_3) &= E_{1F_3} p'^3 p^3 \\
V_{\text{ct}}^{(6)}(3F_3) &= E_{3F_3} p'^3 p^3 \\
V_{\text{ct}}^{(6)}(3F_4) &= E_{3F_4} p'^3 p^3. \tag{2.31}
\end{aligned}$$

To obtain an optimal fit of the NN data at the highest order we consider in this paper, we include the above F -wave contacts in our N⁴LO potentials.

E. Charge dependence

This is to summarize what charge-dependence we include. Through all orders, we take the charge-dependence of the 1PE due to pion-mass splitting into account, Eqs. (2.18) and (2.19). Charge-dependence is seen most prominently in the $1S_0$ state at low energies, particularly, in the $1S_0$ scattering lengths. Charge-dependent 1PE cannot explain it all. The remainder is accounted for by treating the $1S_0$ LO contact parameter, \widetilde{C}_{1S_0} , Eq. (2.25), in a charge-dependent way. Thus, we will distinguish between $\widetilde{C}_{1S_0}^{\text{pp}}$, $\widetilde{C}_{1S_0}^{\text{np}}$, and $\widetilde{C}_{1S_0}^{\text{nn}}$. For pp scattering at any order, we include the relativistic Coulomb potential [61, 62]. Finally, at N³LO and N⁴LO, we take into account irreducible π - γ exchange [63], which affects only the np potential. We also take nucleon-mass splitting into account, or in other words, we always apply the correct values for the masses of the nucleons involved in the various charge-dependent NN potentials.

For a comprehensive discussion of all possible sources for the charge-dependence of the NN interaction, see Ref. [1].

F. The full potential

The sum of long-range [Eqs. (2.12)-(2.16)] plus short-range potentials [Eq. (2.23)] results in:

$$V_{\text{LO}} \equiv V^{(0)} = V_{1\pi} + V_{\text{ct}}^{(0)} \quad (2.32)$$

$$V_{\text{NLO}} \equiv V^{(2)} = V_{\text{LO}} + V_{2\pi}^{(2)} + V_{\text{ct}}^{(2)} \quad (2.33)$$

$$V_{\text{NNLO}} \equiv V^{(3)} = V_{\text{NLO}} + V_{2\pi}^{(3)} \quad (2.34)$$

$$V_{\text{N3LO}} \equiv V^{(4)} = V_{\text{NNLO}} + V_{2\pi}^{(4)} + V_{3\pi}^{(4)} + V_{\text{ct}}^{(4)} \quad (2.35)$$

$$V_{\text{N4LO}} \equiv V^{(5)} = V_{\text{N3LO}} + V_{2\pi}^{(5)} + V_{3\pi}^{(5)}, \quad (2.36)$$

where we left out the higher order corrections to the 1PE because, as discussed, they are absorbed by mass and coupling constant renormalizations. It is also understood that the charge-dependence discussed in the previous subsection is included.

In our systematic potential construction, we follow the above scheme, except for two physically motivated modifications. We add to V_{N3LO} the $1/M_N$ correction of the NNLO 2PE proportional to c_i . This correction is proportional to c_i/M_N and appears nominally at fifth order, because we count $Q/M_N \sim (Q/\Lambda_\chi)^2$. This contribution is given in Eqs. (2.19)-(2.23) of Ref. [52] and we denote it by $V_{2\pi, c_i/M_N}^{(5)}$. In short, in Eq. (2.35), we replace

$$V_{\text{N3LO}} \mapsto V_{\text{N3LO}} + V_{2\pi, c_i/M_N}^{(5)}. \quad (2.37)$$

As demonstrated in Ref. [15], the 2PE bubble diagram proportional to c_i^2 that appears at N³LO is unrealistically attractive, while the c_i/M_N correction is large and repulsive. Therefore, it makes sense to group these diagrams together to arrive at a more realistic intermediate attraction at N³LO.

The second modification consists of adding to V_{N4LO} the four F -wave contacts listed in Eq. (2.31) to ensure an optimal fit of the NN data for the potential of the highest order constructed in this work.

The potential V is, in principal, an invariant amplitude (with relativity taken into account perturbatively) and, thus, satisfies a relativistic scattering equation, like, e. g., the Blankenbeclar-Sugar (BbS) equation [64], which reads explicitly,

$$T(\vec{p}', \vec{p}) = V(\vec{p}', \vec{p}) + \int \frac{d^3 p''}{(2\pi)^3} V(\vec{p}', \vec{p}'') \frac{M_N^2}{E_{p''}} \frac{1}{p^2 - p''^2 + i\epsilon} T(\vec{p}'', \vec{p}) \quad (2.38)$$

with $E_{p''} \equiv \sqrt{M_N^2 + p''^2}$ and M_N the nucleon mass. The advantage of using a relativistic scattering equation is that it automatically includes relativistic kinematical corrections to all orders. Thus, in the scattering equation, no propagator modifications are necessary when moving up to higher orders.

Defining

$$\widehat{V}(\vec{p}', \vec{p}) \equiv \frac{1}{(2\pi)^3} \sqrt{\frac{M_N}{E_{p'}}} V(\vec{p}', \vec{p}) \sqrt{\frac{M_N}{E_p}} \quad (2.39)$$

and

$$\widehat{T}(\vec{p}', \vec{p}) \equiv \frac{1}{(2\pi)^3} \sqrt{\frac{M_N}{E_{p'}}} T(\vec{p}', \vec{p}) \sqrt{\frac{M_N}{E_p}}, \quad (2.40)$$

where the factor $1/(2\pi)^3$ is added for convenience, the BbS equation collapses into the usual, nonrelativistic Lippmann-Schwinger (LS) equation,

$$\widehat{T}(\vec{p}', \vec{p}) = \widehat{V}(\vec{p}', \vec{p}) + \int d^3 p'' \widehat{V}(\vec{p}', \vec{p}'') \frac{M_N}{p^2 - p''^2 + i\epsilon} \widehat{T}(\vec{p}'', \vec{p}). \quad (2.41)$$

Since \widehat{V} satisfies Eq. (2.41), it may be regarded as a nonrelativistic potential. By the same token, \widehat{T} may be considered as the nonrelativistic T-matrix. All technical aspects associated with the solution of the LS equation can be found in Appendix A of Ref. [65], including specific formulas for the calculation of the np and pp phase shifts (with Coulomb). Additional details concerning the relevant operators and their decompositions are given in section 4 of Ref. [66]. Finally, computational methods to solve the LS equation are found in Ref. [67].

G. Regularization and non-perturbative renormalization

Iteration of \widehat{V} in the LS equation, Eq. (2.41), requires cutting \widehat{V} off for high momenta to avoid infinities. This is consistent with the fact that ChPT is a low-momentum expansion which is valid only for momenta $Q < \Lambda_\chi \approx 1$ GeV. Therefore, the potential \widehat{V} is multiplied with the regulator function $f(p', p)$,

$$\widehat{V}(\vec{p}', \vec{p}) \mapsto \widehat{V}(\vec{p}', \vec{p}) f(p', p) \quad (2.42)$$

with

$$f(p', p) = \exp[-(p'/\Lambda)^{2n} - (p/\Lambda)^{2n}], \quad (2.43)$$

such that

$$\widehat{V}(\vec{p}', \vec{p}) f(p', p) \approx \widehat{V}(\vec{p}', \vec{p}) \left\{ 1 - \left[\left(\frac{p'}{\Lambda} \right)^{2n} + \left(\frac{p}{\Lambda} \right)^{2n} \right] + \dots \right\}. \quad (2.44)$$

For the cutoff parameter Λ , we apply three different values, namely, 450, 500, and 550 MeV.

Equation (2.44) provides an indication of the fact that the exponential cutoff does not necessarily affect the given order at which the calculation is conducted. For sufficiently large n , the regulator introduces contributions that are beyond the given order. Assuming a good rate of convergence of the chiral expansion, such orders are small as compared to the given order and, thus, do not affect the accuracy at the given order. Thus, we use $n = 2$ for 3PE and 2PE and $n = 4$ for 1PE (except in LO and NLO, where we use $n = 2$ for 1PE). For contacts of order ν , n is chosen such that $2n > \nu$.

In our calculations, we apply, of course, the exponential form, Eq. (2.43), and not the expansion Eq. (2.44). On a similar note, we also do not expand the square-root factors in Eqs. (2.39-2.40) because they are kinematical factors which guarantee relativistic elastic unitarity.

It is pretty obvious that results for the T -matrix may depend sensitively on the regulator and its cutoff parameter. The removal of such regulator dependence is known as renormalization.

The renormalization of the *perturbatively* calculated NN potential is not a problem. *The problem is nonperturbative renormalization.* This problem typically occurs in *nuclear* EFT because nuclear physics is characterized by bound states and large scattering length which are nonperturbative in nature. Or in other words, to obtain the nuclear amplitude, the potential has to be resummed (to infinite orders) in the LS equation Eq. (2.41). EFT power counting may be different for nonperturbative processes as compared to perturbative ones. Such difference may be caused by the infrared enhancement of the reducible diagrams generated in the LS equation.

Weinberg's implicit assumption [5] was that the counterterms introduced to renormalize the perturbatively calculated potential, based upon naive dimensional analysis ("Weinberg counting", cf. Sec. II B), are also sufficient to renormalize the nonperturbative resummation of the potential in the LS equation.

Weinberg's assumption may not be correct as first pointed out by Kaplan, Savage, and Wise [68], and we like to refer the interested reader to Section 4.5 of Ref. [1] for a comprehensive discussion of the issue. Even today, no generally accepted solution to this problem has emerged and some more recent proposals can be found in Refs. [69–76]. Concerning the construction of quantitative NN potential (by which we mean NN potentials suitable for use in contemporary many-body nuclear methods), only Weinberg counting has been used with success during the past 25 years [1, 6, 17, 21, 23, 26], which is why also in the present work we will apply Weinberg counting.

In spite of the criticism, Weinberg counting may be perceived as not unreasonable by the following argument. For a successful EFT (in its domain of validity), one must be able to claim independence of the predictions on the regulator within the theoretical error. Also, truncation errors must decrease as we go to higher and higher orders. These are precisely the goals of renormalization.

Lepage [77] has stressed that the cutoff independence should be examined for cutoffs below the hard scale and not beyond. Ranges of cutoff independence within the theoretical error are to be identified using Lepage plots [77]. A systematic investigation of this kind has been conducted in Ref. [78]. In that work, the error of the predictions was quantified by calculating the χ^2/datum for the reproduction of the np elastic scattering data as a function of the cutoff parameter Λ of the regulator function Eq. (2.43). Predictions by chiral np potentials at order NLO and NNLO were investigated applying Weinberg counting for the counter terms (NN contact terms). It is found that the reproduction of the np data at lab. energies below 200 MeV is generally poor at NLO, while at NNLO the χ^2/datum assumes acceptable values (a clear demonstration of order-by-order improvement). Moreover, at NNLO, a "plateau" of constant low χ^2 for cutoff parameters ranging from about 450 to 850 MeV can be identified. This may be perceived as cutoff independence (and, thus, successful renormalization) for the relevant range of cutoff parameters.

TABLE III: Publication history of the NN data below 350 MeV laboratory energy and references for their listings. Only data that pass the Nijmegen acceptance criteria [62] are counted. ‘Total’ defines the 2016 database.

Publication date	No. of pp data	No. of np data	References
Jan. 1955 – Dec. 1992	1787	2514	[79, 80]
Jan. 1993 – Dec. 1999	1145	544	Tables XV and XVI of Ref. [65]
Jan. 2000 – Dec. 2016	140	511	Ref. [83] and Table IV of present paper
Total	3072	3569	

III. NN SCATTERING AND THE DEUTERON

Based upon the formalism presented in the previous section, we have constructed NN potentials through five orders of the chiral expansion, ranging from LO (Q^0) to N^4 LO (Q^5). In each order, we consider three cutoffs, namely, $\Lambda = 450, 500, \text{ and } 550$ MeV. Since we take charge-dependence into account, each NN potential comes in three versions: pp , np , and nn . The results from these potentials for NN scattering and the deuteron will be presented in this section.

A. NN database

Since an important part of NN potential construction involves optimizing the reproduction of the NN data by the potential, we need to state, first, what NN database we are using.

Our database consists of all NN data below 350 MeV laboratory energy published in refereed physics journals between January 1955 and December 2016 that are not discarded when applying the Nijmegen rejection criteria [62]. We will refer to this as the ‘‘2016 database’’. This database was started by the Nijmegen group who critically checked and assembled the data published up to December 1992. This 1992 database consists of 1787 pp data (listed in Ref. [79]) and 2514 np data (tabulated in Ref. [80]), cf. Table III. In Ref. [65], the database was then extended to include the data published up to December 1999 that survived the Nijmegen rejection criteria. This added 1145 pp and 544 np data (given in Tables XV and XVI of Ref. [65], respectively). Thus, the 1999 database includes 2932 pp and 3058 np data.

To get to the 2016 database, we have added to the 1999 database the data published between January 2000 and December 2016 that are not rejected by the Nijmegen criteria. We are aware of the fact that modified rejection criteria have been proposed [81] and applied in recent NN data analysis work [82]. But we continue to apply the classic Nijmegen criteria [62] to be consistent with the pre-2000 part of the database.

Concerning after-1999 pp data, there exists only one set of 139 differential cross sections between 239.9 and 336.2 MeV measured by the EDDA group at COSY (J ulich, Germany) with an over-all uncertainty of 2.5% [83]. Thus, the total number of pp data contained in the 2016 database is 3072 (Table III).

In contrast to pp , there have been many new np measurements after 1999. We list the datasets that survived the Nijmegen rejection criteria in Table IV. According to that list, the number of valid after-1999 np data is 511, bringing the total number of np data contained in the 2016 database to 3569 (Table III).

For comparison, we mention that the 2013 Granada NN database [82] consists of 2996 pp and 3717 np data. The larger number of pp data in our base is mainly due to the inclusion of 140 pp data from Ref. [83] which are left out in the Granada base. On the other hand, the Granada base contains 148 more np data which is a consequence of the modified rejection criteria applied by the Granada group which allows for the survival of more np data.

Finally, we note that in the potential construction reported in this paper, we make use of the 2016 database only up to 290 MeV laboratory energy (pion-production threshold). Between 0 and 290 MeV, the 2016 database contains 2132 pp data and 2721 np data (cf. Table V).

B. Data fitting procedure

When we are talking about data fitting, we are referring to the adjustment of the NN contact parameters available at the respective order. Note that in our NN potential construction, the πN LECs are not fit-parameters. The πN LECs are held fixed at their values determined in the πN analysis of Ref. [60] displayed in Table II (we use the central values shown in that Table). Thus, the NN contacts (Sec. IID) are the only fit parameters used to optimize the reproduction of the NN data below 290 MeV laboratory energy. As discussed, those contact terms describe the short-range part of the NN potentials and adjust the lower partial waves.

TABLE IV: After-1999 np data below 350 MeV included in the 2016 np database. ‘‘Error’’ refers to the experimental over-all normalization errors of the individual datasets. ‘None’ signifies that the respective experimental data set does not carry a normalization error, i.e., the data are absolute. ‘Float’ indicates that, in the analysis of the data set, the normalization was allowed to assume a value for which the χ^2 is a minimum disregarding a comparison with the experimental normalization error. This is done in case where there is doubt about the alleged experimental normalization error. In the cases of ‘None’ and ‘Float’, the normalization is not counted as an observable. This table contains 473 observables plus 38 normalizations resulting in a total of 511 data. For the observables, we use in general the notation of Hoshizaki [84], except for types which are undefined in the Hoshizaki formalism, where we use the Saclay notation [85].

T_{lab} (MeV)	No. type	Error (%)	Institution	Ref.
9.2–349.0	92 σ_{tot}	None	Los Alamos	[86]
10.0	6 σ	0.8	Ohio	[87]
95.0	10 σ	5.0	Uppsala	[88]
95.0	9 σ	4.0	Uppsala	[89]
96.0	11 σ	5.0	Uppsala	[90]
96.0	9 σ	3.0	Uppsala	[91]
96.0	12 σ	None	Uppsala	[92]
260.0	8 P	1.8	PSI	[93]
260.0	16 P	1.8	PSI	[93]
260.0	8 A_{yy}	3.9	PSI	[93]
260.0	16 A_{yy}	3.9	PSI	[93]
260.0	9 A_{zz}	7.2	PSI	[93]
260.0	5 D	2.4	PSI	[94]
260.0	8 D	Float	PSI	[94]
260.0	8 $D_{0s''0k}$	Float	PSI	[94]
260.0	5 D_t	2.4	PSI	[94]
260.0	4 A_t	2.4	PSI	[94]
260.0	8 A_t	2.4	PSI	[94]
260.0	4 R_t	2.4	PSI	[94]
260.0	8 R_t	2.4	PSI	[94]
260.0	8 N_{0nkk}	2.4	PSI	[94]
260.0	4 $N_{0s''kn}$	2.4	PSI	[94]
260.0	8 $N_{0s''kn}$	2.4	PSI	[94]
260.0	4 $N_{0s''sn}$	2.4	PSI	[94]
260.0	8 $N_{0s''sn}$	2.4	PSI	[94]
284.0	14 P	3.0	PSI	[95]
314.0	14 P	3.0	PSI	[95]
315.0	16 P	1.2	PSI	[93]
315.0	11 A_{yy}	3.7	PSI	[93]
315.0	16 A_{yy}	3.7	PSI	[93]
315.0	11 A_{zz}	7.1	PSI	[93]
315.0	6 D	Float	PSI	[94]
315.0	6 $D_{0s''0k}$	Float	PSI	[94]
315.0	8 $D_{0s''0k}$	Float	PSI	[94]
315.0	6 D_t	1.9	PSI	[94]
315.0	6 A_t	1.9	PSI	[94]
315.0	8 A_t	1.9	PSI	[94]
315.0	6 R_t	1.9	PSI	[94]
315.0	8 R_t	1.9	PSI	[94]
315.0	5 $N_{0s''kn}$	1.9	PSI	[94]
315.0	8 $N_{0s''kn}$	1.9	PSI	[94]
315.0	6 $N_{0s''sn}$	1.9	PSI	[94]
315.0	8 $N_{0s''sn}$	1.9	PSI	[94]
315.0	8 N_{0nkk}	1.9	PSI	[94]
344.0	14 P	3.0	PSI	[95]

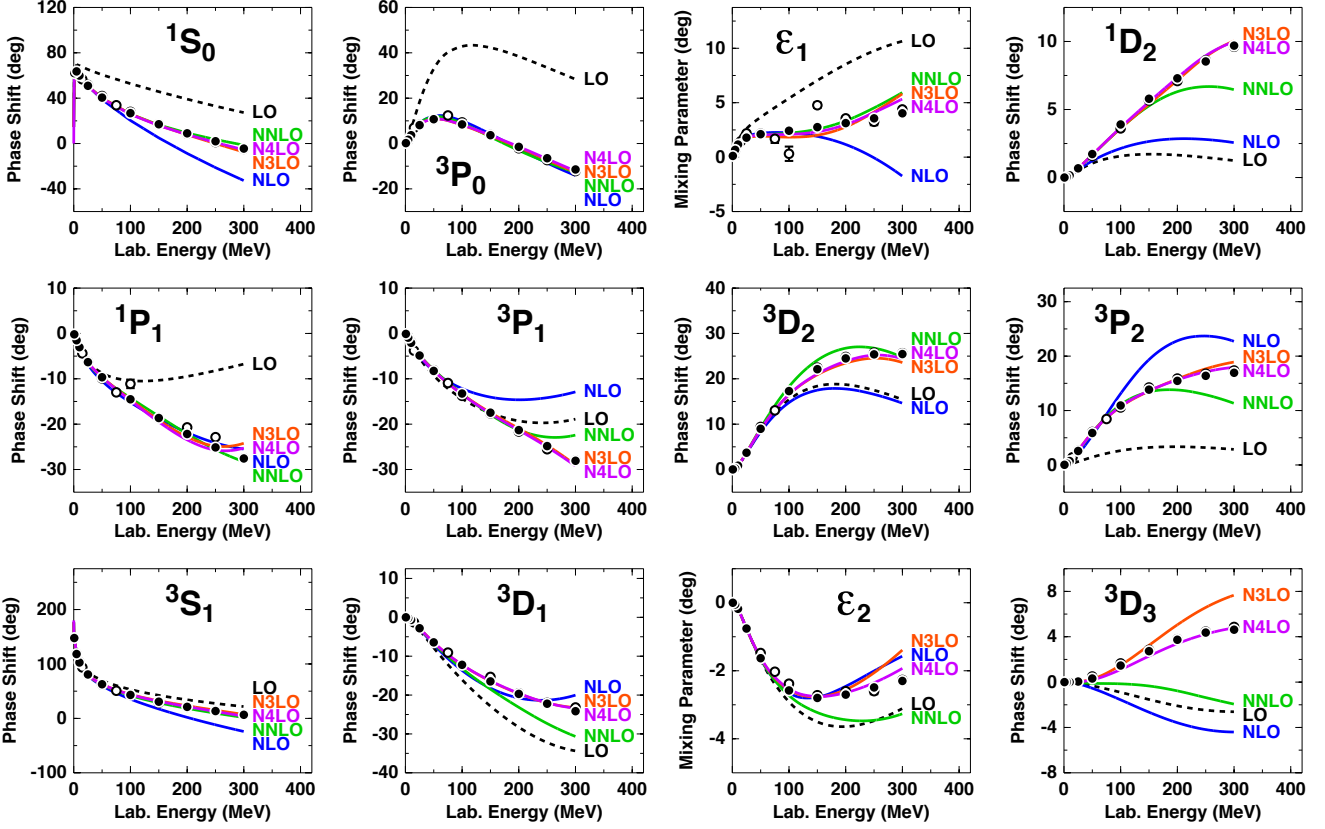


FIG. 2: (Color online). Chiral expansion of neutron-proton scattering as represented by the phase shifts in S , P , and D waves and mixing parameters ϵ_1 and ϵ_2 . Five orders ranging from LO to N^4 LO are shown as denoted. A cutoff $\Lambda = 500$ MeV is applied in all cases. The filled and open circles represent the results from the Nijmegen multi-energy np phase-shift analysis [80] and the GWU single-energy np analysis SP07 [100], respectively.

In the construction of any NN potential, we always start with the pp version since the pp data are the most accurate ones. The fitting is done in three steps. In the first step, the pp potential is adjusted to reproduce as closely as possible the pp phase shifts of the Nijmegen multienergy pp phase shift analysis [80] up to 300 MeV laboratory energy. This is to ensure that phase shifts are in the right ballpark. In the second step, we make use of the Nijmegen pp error matrix [96] to minimize the χ^2 that results from it. The advantage of this step is that it is computationally very fast and easy. Finally, in the third and final step, the pp potential contact parameters are fine-tuned by minimizing the χ^2 that results from a direct comparison with the experimental pp data contained in the 2016 database below 290 MeV. For this we use a copy of the SAID software package which includes all electromagnetic contributions necessary for the calculation of NN observables at low energy. Since it turned out that the Nijmegen error matrix produces very accurate χ^2 for pp energies below 75 MeV, we use the values from this error matrix for the energies up to 75 MeV and the values from a direct confrontation with the data above that energy.

The $I = 1$ np potential is constructed by starting from the pp version, applying the charge-dependence discussed in Sec. II E, and adjusting the non-derivative 1S_0 contact such as to reproduce the 1S_0 np scattering length. This then yields the preliminary fit of the $I = 1$ np potential. The preliminary fit of the $I = 0$ np potential is obtained by a fit to the $I = 0$ np phase shifts of the Nijmegen multienergy np phase shift analysis [80] below 300 MeV. Starting from this preliminary np fit, the contact parameters are fine-tuned in a confrontation with the np data below 290 MeV, for which the χ^2 is minimized. We note that during this last step we have also allowed for minor changes of the $I = 1$ parameters (which also modifies the pp potential) to obtain an even lower χ^2 over-all.

Finally the nn potential is obtained by starting from the pp version, replacing the proton masses by neutron masses, leaving out Coulomb, and adjusting the non-derivative 1S_0 contact such as to reproduce the 1S_0 nn scattering length for which we assume the empirical value of -18.95 MeV [103, 104].

We note that our procedure for fitting NN potentials to data is essentially the same that was used to fit the high-precision NN potentials of the 1990's [65, 97, 98] (fitted up to 350 MeV), and the first precision chiral NN

TABLE V: χ^2/datum for the fit of the 2016 NN data base by NN potentials at various orders of chiral EFT ($\Lambda = 500$ MeV in all cases).

T_{lab} bin (MeV)	No. of data	LO	NLO	NNLO	N ³ LO	N ⁴ LO
proton-proton						
0–100	795	520	18.9	2.28	1.18	1.09
0–190	1206	430	43.6	4.64	1.69	1.12
0–290	2132	360	70.8	7.60	2.09	1.21
neutron-proton						
0–100	1180	114	7.2	1.38	0.93	0.94
0–190	1697	96	23.1	2.29	1.10	1.06
0–290	2721	94	36.7	5.28	1.27	1.10
pp plus np						
0–100	1975	283	11.9	1.74	1.03	1.00
0–190	2903	235	31.6	3.27	1.35	1.08
0–290	4853	206	51.5	6.30	1.63	1.15

TABLE VI: Scattering lengths (a) and effective ranges (r) in units of fm as predicted by NN potentials at various orders of chiral EFT ($\Lambda = 500$ MeV in all cases). (a_{pp}^C and r_{pp}^C refer to the pp parameters in the presence of the Coulomb force. a^N and r^N denote parameters determined from the nuclear force only and with all electromagnetic effects omitted.) a_{nn}^N , and a_{np} are fitted, all other quantities are predictions.

	LO	NLO	NNLO	N ³ LO	N ⁴ LO	Empirical
1S_0						
a_{pp}^C	-7.8153	-7.8128	-7.8140	-7.8155	-7.8160	-7.8196(26) [62] -7.8149(29) [102]
r_{pp}^C	1.886	2.678	2.758	2.772	2.774	2.790(14) [62] 2.769(14) [102]
a_{pp}^N	—	-17.476	-17.762	-17.052	-17.123	—
r_{pp}^N	—	2.752	2.821	2.851	2.853	—
a_{nn}^N	-18.950	-18.950	-18.950	-18.950	-18.950	-18.95(40) [103, 104]
r_{nn}^N	1.857	2.726	2.800	2.812	2.816	2.75(11) [105]
a_{np}	-23.738	-23.738	-23.738	-23.738	-23.738	-23.740(20) [65]
r_{np}	1.764	2.620	2.687	2.700	2.704	[2.77(5)] [65]
3S_1						
a_t	5.255	5.415	5.418	5.420	5.420	5.419(7) [65]
r_t	1.521	1.755	1.752	1.754	1.753	1.753(8) [65]

potentials [1, 16] (fitted up to 290 MeV). This is quite in contrast to the procedure applied in the recent construction of the NNLO_{sat} potential [26], where the NN data up to 35 MeV and the groundstate energies and radii of nuclei up to ^{40}Ca are taken into account to fix simultaneously the 2NF and 3NF. In Ref. [26], the NN data up to 35 MeV are reproduced with a χ^2/datum of 4.3. Similar procedures are applied in Ref. [27].

Our fit procedures differ also substantially from the ones used in the recent chiral NN potential constructions of Refs [23, 24], where the potentials are fitted to phase shifts. Already in the early 1990’s, the Nijmegen group has pointed out repeatedly and demonstrated clearly [96], that fitting to experimental data should be preferred over fitting to phase shifts, because a seemingly “good” fit to phase shifts can result in a bad reproduction of the data. Note that phase shifts are not experimental data.

TABLE VII: Two- and three-nucleon bound-state properties as predicted by NN potentials at various orders of chiral EFT ($\Lambda = 500$ MeV in all cases). (Deuteron: Binding energy B_d , asymptotic S state A_S , asymptotic D/S state η , structure radius r_{str} , quadrupole moment Q , D -state probability P_D ; the predicted r_{str} and Q are without meson-exchange current contributions and relativistic corrections. Triton: Binding energy B_t .) B_d is fitted, all other quantities are predictions.

	LO	NLO	NNLO	N ³ LO	N ⁴ LO	Empirical ^a
Deuteron						
B_d (MeV)	2.224575	2.224575	2.224575	2.224575	2.224575	2.224575(9)
A_S (fm ^{-1/2})	0.8526	0.8828	0.8844	0.8853	0.8852	0.8846(9)
η	0.0302	0.0262	0.0257	0.0257	0.0258	0.0256(4)
r_{str} (fm)	1.911	1.971	1.968	1.970	1.973	1.97507(78)
Q (fm ²)	0.310	0.273	0.273	0.271	0.273	0.2859(3)
P_D (%)	7.29	3.40	4.49	4.15	4.10	—
Triton						
B_t (MeV)	11.09	8.31	8.21	8.09	8.08	8.48

^aSee Table XVIII of Ref. [65] for references; the empirical value for r_{str} is from Ref. [106].

C. Results for NN scattering

The χ^2/datum for the reproduction of the NN data at various orders of chiral EFT are shown in Table V for different energy intervals below 290 MeV laboratory energy (T_{lab}). The bottom line of Table V summarizes the essential results. For the close to 5000 pp plus np data below 290 MeV (pion-production threshold), the χ^2/datum is 51.4 at NLO and 6.3 at NNLO. Note that the number of NN contact terms is the same for both orders. The improvement is entirely due to an improved description of the 2PE contribution, which is responsible for the crucial intermediate-range attraction of the nuclear force. At NLO, only the uncorrelated 2PE is taken into account which is insufficient. From the classic meson-theory of nuclear forces [99], it is wellknown that π - π correlations and nucleon resonances need to be taken into account for a realistic model of 2PE that provides a sufficient amount of intermediate attraction to properly bind nucleons in nuclei. In the chiral theory, these contributions are encoded in the subleading πN vertexes with LECs denoted by c_i . These enter at NNLO and are the reason for the substantial improvements we encounter at that order. This is the best proof that, starting at NNLO, the chiral approach to nuclear forces is getting the physics right.

To continue on the bottom line of Table V, after NNLO, the χ^2/datum then further improves to 1.63 at N³LO and, finally, reaches the almost perfect value of 1.15 at N⁴LO—a fantastic convergence.

Corresponding np phase shifts are displayed in Fig. 2, which reflect what the χ^2 have already proven, namely, an excellent convergence when going from NNLO to N³LO and, finally, to N⁴LO. However, at LO and NLO there are large discrepancies between the predictions and the empirical phase shifts as to be expected from the corresponding χ^2 values. This fact renders applications of the LO and NLO nuclear force useless for any realistic calculation (but they could be used to demonstrate truncation errors).

For order N⁴LO (with $\Lambda = 500$ MeV), we also provide the numerical values for the phase shifts in Appendix A. Our pp phase shifts are the phase shifts of the nuclear plus relativistic Coulomb interaction with respect to Coulomb wave functions. Note, however, that for the calculation of observables (e.g., to obtain the χ^2 in regard to experimental data), we use electromagnetic phase shifts, as *necessary*, which we obtain by adding to the Coulomb phase shifts the effects from two-photon exchange, vacuum polarization, and magnetic moment interactions as calculated by the Nijmegen group [62, 101]. This is important for 1S_0 below 30 MeV and negligible otherwise. For nn and np scattering, our phase shifts are the ones from the nuclear interaction with respect to Riccati-Bessel functions. The technical details of our phase shift calculations can be found in appendix A3 of Ref. [65].

The low-energy scattering parameters, order by order, are shown in Table VI. For nn and np , the effective range expansion without any electromagnetic interaction is used. In the case of pp scattering, the quantities a_{pp}^C and r_{pp}^C are obtained by using the effective range expansion appropriate in the presence of the Coulomb force (cf. appendix A4 of Ref. [65]). Note that the empirical values for a_{pp}^C and r_{pp}^C in Table VI were obtained by subtracting from the corresponding electromagnetic values the effects due to two-photon exchange and vacuum polarization. Thus, the comparison between theory and experiment for these two quantities is conducted correctly. a_{nn}^N , and a_{np} are fitted, all other quantities are predictions. Note that the 3S_1 effective range parameters a_t and r_t are not fitted. But the deuteron binding energy is fitted (cf. next subsection) and that essentially fixes a_t and r_t .

TABLE VIII: χ^2/datum for the fit of the pp plus np data up to 190 MeV and two- and three-nucleon bound-state properties as produced by NN potentials at NNLO and N⁴LO applying different values for the cutoff parameter Λ of the regulator function Eq. (2.43). For some of the notation, see Table VII, where also empirical information on the deuteron and triton can be found.

$\Lambda(\text{MeV})$	NNLO			N ⁴ LO		
	450	500	550	450	500	550
$\chi^2/\text{datum } pp \ \& \ np$						
0–190 MeV (2903 data)	4.12	3.27	3.32	1.17	1.08	1.25
Deuteron						
B_d (MeV)	2.224575	2.224575	2.224575	2.224575	2.224575	2.224575
A_S (fm ^{-1/2})	0.8847	0.8844	0.8843	0.8852	0.8852	0.8851
η	0.0255	0.0257	0.0258	0.0254	0.0258	0.0257
r_{str} (fm)	1.967	1.968	1.968	1.966	1.973	1.971
Q (fm ²)	0.269	0.273	0.275	0.269	0.273	0.271
P_D (%)	3.95	4.49	4.87	4.38	4.10	4.13
Triton						
B_t (MeV)	8.35	8.21	8.10	8.04	8.08	8.12

D. Deuteron and triton

The evolution of the deuteron properties from LO to N⁴LO of chiral EFT are shown in Table VII. In all cases, we fit the deuteron binding energy to its empirical value of 2.224575 MeV using the non-derivative 3S_1 contact. All other deuteron properties are predictions. Already at NNLO, the deuteron has converged to its empirical properties and stays there through the higher orders.

At the bottom of Table VII, we also show the predictions for the triton binding as obtained in 34-channel charge-dependent Faddeev calculations using only 2NFs. The results show smooth and steady convergence, order by order, towards a value around 8.1 MeV that is reached at the highest orders shown. This contribution from the 2NF will require only a moderate 3NF. The relatively low deuteron D -state probabilities ($\approx 4.1\%$ at N³LO and N⁴LO) and the concomitant generous triton binding energy predictions are a reflection of the fact that our NN potentials are soft (which is, at least in part, due to their non-local character).

E. Cutoff variations

As noted before, besides the case $\Lambda = 500$ MeV, we have also constructed potentials with $\Lambda = 450$ and 550 MeV at each order, to allow for systematic studies of the cutoff dependence. In Fig. 3, we display the variations of the np phase shifts for different cutoffs at NNLO (left half of figure, green curves) and at N⁴LO (right half of figure, purple curves). We do not show the cutoff variations of phase shifts at N³LO, because they are about the same as at N⁴LO. Similarly, the variations at NLO are of about the same size as at NNLO. Fig. 3 demonstrates nicely how cutoff dependence diminishes with increasing order—a reasonable trend. Another point that is evident from this figure is that $\Lambda = 450$ MeV should be considered as a lower limit for cutoffs, because obviously cutoff artifacts start showing up—above 200 MeV, particularly, in 1D_2 and 3D_2 . Concerning the upper limit for the cutoff: It has been discussed and demonstrated in length in the literature (see, e.g., Ref. [23]) that for the NN interaction the breakdown scale occurs around $\Lambda_b \approx 600$ MeV. The motivation for our upper value of 550 MeV is to stay below Λ_b .

In Table VIII, we show the cutoff dependence for three selected aspects that are of great interest: the χ^2 for the fit of the NN data below 190 MeV, the deuteron properties, and the triton binding energy. The χ^2 does not change substantially as a function of cutoff, and crucial deuteron properties, like A_S and η , stay within the empirical range, for both NNLO and N⁴LO. Thus, we can make the interesting observation that the reproduction of NN observables is not much affected by the cutoff variations. However, the D -state probability of the deuteron, P_D , which is not an observable, changes substantially as a function of cutoff at NNLO (namely, by $\approx 1\%$) while it changes only by 0.25% at N⁴LO. Note that P_D is intimately related to the off-shell behavior of a potential and so are the binding energies of few-body systems. Therefore, in tune with the P_D variations, the binding energy of the triton varies by 0.25 MeV at NNLO, while it changes only by 0.08 MeV at N⁴LO. In this context, it is of interest to note that changes in the

TABLE IX: Effective πN LECs (in units of GeV^{-1}) recommended for the 2PE 3NF at the given orders. See text for explanations.

	NNLO	N ³ LO	N ⁴ LO
\bar{c}_1	-0.74	-1.20	-0.73
\bar{c}_3	-3.61	-4.43	-3.38
\bar{c}_4	2.44	2.67	1.69

off-shell behavior of the 2NF can be compensated by corresponding changes in the 3NF, as demonstrated by Polyzou and Glöcke [107].

Even though cutoff variations are, in general, not the most reliable way to estimate truncation errors, in the above case they seem to reflect closely what we expect to be the truncation error.

IV. CHIRAL THREE-BODY FORCES

As is well established, realistic *ab initio* nuclear structure calculations require the inclusion of 3NFs (and potentially also four-nucleon forces). The first 3NFs occur at NNLO (cf. Fig. 1) and were derived in Refs. [31, 108]. The 3NFs at N³LO can be found in Refs. [109, 110]. Finally, at N⁴LO, the longest-range and intermediate-range 3NFs are given in Refs. [46, 47]. Moreover, a new set of ten 3NF contact terms occurs at N⁴LO, which has been derived by the Pisa group [49]. An efficient approach for calculating the matrix elements of chiral 3NF contributions up to N³LO has been published in Ref. [111]. This approach may eventually be extended to N⁴LO.

In the derivation of all of the above-cited chiral 3NFs, the same power-counting scheme is applied as in the derivation of the 2NFs of this paper, namely, Weinberg counting and considering $Q/M_N \sim (Q/\Lambda_\chi)^2$ (Sec. IIB). Thus, those 3NF expressions are consistent with the present 2NFs, and they can be used together in *ab initio* calculations of nuclear structure and reactions.

In this context it is worth noting that, for convenience, the 3NFs are derived using dimensional regularization (DR), while we use SFR in the construction of the 2NFs [cf. Eq. (2.22)]. This is, however, not a problem because, as shown in Ref. [58], DR and SFR expressions differ only by higher order terms that are beyond the given order. Thus, the accuracy of the calculation conducted at a given order is not affected. An equivalent argument applies to the use of nonlocal regulators [Eq. (2.43)] *versus* local ones (e.g., Eq. (11) of Ref. [18]), since also these two types of regulators differ only by higher order terms beyond the given order.

Because of the complexity of the N⁴LO 3NF, it may still take a few years until this force is available in a manageable form. Thus, for a while, we will have to live with incomplete calculations. However, there is one important component of the 3NF where, indeed, complete calculations up to N⁴LO are possible: it is the 2PE 3NF. In Ref. [46] it has been shown that the 2PE 3NF has essentially the same mathematical structure at NNLO, N³LO, and N⁴LO. Thus, one can add up the three orders of 3NF contributions and parametrize the result in terms of effective LECs. This was done in Ref. [46] and we show the effective LECs they come up with in Table IX, column N⁴LO, where we quote the numbers given in Eq. (5.2) of Ref. [46], which are based upon the GW πN phase shifts [112]. Note that the LECs of Ref. [60], which we are using for the 2NF, are also based upon GW input. Thus, there is consistency between the effective \bar{c}_i for the 3NF (column N⁴LO of Table IX) and our c_i for the 2NF (column N⁴LO of Table II).

Concerning, the 2PE 3NF at N³LO, Eq. (2.8) of Ref. [109] provides the corrections to the c_i when the 2PE 3NF at N³LO is added in. Note, however, that there is a error in the numerical values given below Eq. (2.8) of Ref. [109]. While $\delta c_1 = -0.13 \text{ GeV}^{-1}$ is correct, the correct values for δc_3 and δc_4 are $\delta c_3 = -\delta c_4 = 0.89 \text{ GeV}^{-1}$. When these corrections are applied to the N³LO c_i of our Table II, then the values given in the N³LO column of Table IX emerge. By using the \bar{c}_i of Table IX in the mathematical expression of the NNLO 3NF, one can include at least the 2PE parts of the 3NF up to N³LO and even up to N⁴LO in a straightforward way.

The 2PE 3NF is the most obvious among all possible 3NF contributions. Historically, it is the first 3NF ever calculated [113]. The above-given prescriptions allow to take care of this very basic 3NF up to the highest orders considered in this paper.

V. UNCERTAINTY QUANTIFICATIONS

When applying chiral two- and many-body forces in *ab initio* calculations producing predictions for observables of nuclear structure and reactions, major sources of uncertainties are [54]:

1. Experimental errors of the input NN data that the 2NFs are based upon and the input few-nucleon data to which the 3NFs are adjusted.
2. Uncertainties in the Hamiltonian due to
 - (a) uncertainties in the determination of the NN and $3N$ contact LECs,
 - (b) uncertainties in the πN LECs,
 - (c) regulator dependence,
 - (d) EFT truncation error.
3. Uncertainties associated with the few- and many-body methods applied.

The experimental errors in the NN scattering and deuteron data propagate into the NN potentials that are adjusted to reproduce those data. To systematically investigate this error propagation, the Granada group has constructed smooth local potentials [114], the parameters of which carry the uncertainties implied by the errors in the NN data. Applying 205 Monte Carlo samples of these potentials, they find an uncertainty of 15 keV for the triton binding energy [115]. In a more recent study [116], in which only 33 Monte Carlo samples were used, the Granada group reproduced the uncertainty of 15 keV for the triton binding energy and, in addition, determined the uncertainty for the ${}^4\text{He}$ binding energy to be 55 keV. The conclusion is that the statistical error propagation from the NN input data to the binding energies of light nuclei is negligible as compared to uncertainties from other sources (discussed below). Thus, this source of error can be safely neglected at this time. Furthermore, we need to consider the propagation of experimental errors from the experimental few-nucleon data that the 3NF contact terms are fitted to. Also this will be negligible as long as the 3NFs are adjusted to data with very small experimental errors; for example the empirical binding energy of the triton is 8.481795 ± 0.000002 MeV, which will definitely lead to negligible propagation.

Now turning to the Hamiltonian, we have to, first, account for uncertainties in the NN and $3N$ LECs due to the way they are fixed. Based upon our experiences from Ref. [78] and the fact that chiral EFT is a low-energy expansion, we have fitted the NN contact LECs to the NN data below 100 MeV at LO and NLO, below 190 MeV at NNLO, and below 290 MeV at $N^3\text{LO}$ and $N^4\text{LO}$. One could think of choosing these fit-intervals slightly different and a systematic investigation of the impact of such variation on the NN LECs is still outstanding. However, we do not anticipate that large uncertainties would emerge from this source of error.

The story is different for the 3NF contact LECs, since several, very different procedures are in use for how to fix, e. g., the two contact parameters of the NNLO 3NF, known as the c_D and c_E parameters (and once the ten 3NF contacts at $N^4\text{LO}$ come into play, the situation will be even more divers). Since, at NNLO, two parameters have to be fixed, two data are needed. In most procedures, one of them is the triton binding energy. For the second datum, the following choices have been made: the nd doublet scattering length ${}^2a_{nd}$ [31], the binding energy of ${}^4\text{He}$ [117], the point charge radius radius of ${}^4\text{He}$ [40], the Gamow-Teller matrix element of tritium β -decay [118–120]. Alternatively, the c_D and c_E parameters have also been pinned down by just an optimal over-all fit of the properties of light nuclei [121]. 3NF contact LECs determined by different procedures will lead to different predictions for the observables that were not involved in the fitting procedure. The differences in those results establish the uncertainty. Specifically, it would be of interest to investigate the differences that occur for the properties of intermediate-mass nuclei and nuclear matter when 3NF LECs fixed by different protocols are applied.

The uncertainty in the πN LECs used to be a large source of uncertainty, in particular, for predictions for many-body systems [122–124]. With the new, high-precision determination of the πN LECs in the Roy-Steiner equations analysis [60] (cf. Table II) this large uncertainty is essentially eliminated, which is great progress, since it substantially reduces the error budget. We have varied the πN LECs within the errors given in Table II and find that the changes caused by these variations can easily be compensated by small readjustments of the NN LECs resulting in essentially identical phase shifts and χ^2 for the fit of the data. Thus, this source of error is essentially negligible. The πN LECs also appear in the 3NFs, which also include contacts that can be used for readjustment. Future calculations of finite nuclei and nuclear matter should investigate what residual changes remain after such readjustment (that would represent the uncertainty). We expect this to be small.

The choice of the regulator function and its cutoff parameter create uncertainty. Originally, cutoff variations were perceived as a demonstration of the uncertainty at a given order (equivalent to the truncation error). However, in various investigations [23, 44] it has been demonstrated that this is not correct and that cutoff variations, in general, underestimate this uncertainty. Therefore, the truncation error is better determined by sticking literally to what ‘truncation error’ means, namely, the error due to ignoring contributions from orders beyond the given order ν . The largest such contribution is the one of order $(\nu + 1)$, which one may, therefore, consider as representative for the magnitude of what is left out. This suggests that the truncation error at order ν can reasonably be defined as

$$\Delta X_\nu = |X_\nu - X_{\nu+1}|, \quad (5.1)$$

where X_ν denotes the prediction for observable X at order ν . If $X_{\nu+1}$ is not available, then one may use,

$$\Delta X_\nu = |X_{\nu-1} - X_\nu|Q/\Lambda, \quad (5.2)$$

choosing a typical value for the momentum Q , or $Q = m_\pi$. Alternatively, one may also apply more elaborate definitions, like the one given in Ref. [23]. Note that one should not add up (in quadrature) the uncertainties due to regulator dependence and the truncation error, because they are not independent. In fact, it is appropriate to leave out the uncertainty due to regulator dependence entirely and just focus on the truncation error [23]. The latter should be estimated using the same cutoff (e. g., $\Lambda = 500$ MeV) in all orders considered.

Finally, the last uncertainty to be taken into account is the uncertainty in the few- and many-body methods applied in the *ab initio* calculation. This source of error has nothing to do with EFT. Few-body problems are nowadays exactly solvable such that the error is negligible in those cases. For heavier nuclei and nuclear matter, there are definitely uncertainties no matter what method is used. These uncertainties need to be estimated by the practitioners of those methods. But with the improvements of algorithms and the increase of computing power these errors are decreasing.

The bottom line is that the most substantial uncertainty is the truncation error. This is the dominant source of (systematic) error that should be carefully estimated for any calculation applying chiral 2NFs and 3NFs up to a given order.

VI. SUMMARY AND CONCLUSIONS

We have constructed chiral NN potentials through five orders of chiral EFT ranging from LO to N⁴LO [125]. The construction may be perceived as consistent, because the same power counting scheme as well as the same cutoff procedures are applied in all orders. Moreover, the long-range part of these potentials are fixed by the very accurate πN LECs as determined in the Roy-Steiner equations analysis of Ref. [60]. In fact, the uncertainties of these LECs are so small that a variation within the errors leads to effects that are essentially negligible at the current level of precision. Another aspect that has to do with precision is that, at least at the highest order (N⁴LO), the NN data below pion-production threshold are reproduced with the outstanding χ^2/datum of 1.15. This is the highest precision ever accomplished with any chiral NN potential to date.

The NN potentials presented in this paper may serve as a solid basis for systematic *ab initio* calculations of nuclear structure and reactions that allow for a comprehensive error analysis. In particular, the order by order development of the potentials will make possible a reliable determination of the truncation error at each order.

Our family of potentials is non-local and, generally, of soft character. This feature is reflected in the fact that the predictions for the triton binding energy (from two-body forces only) converges to about 8.1 MeV at the highest orders. This leaves room for moderate three-nucleon forces.

These features of our potentials are in contrast to other families of chiral NN potentials of local or semi-local character that have recently entered the market [20–24]. Such potentials are less soft and, consequently, require stronger three-body force contributions.

The availability of families of chiral NN potentials of different character offers the opportunity for interesting systematic studies that may ultimately shed light on issues, like, the “radius problem” [50], the overbinding of intermediate-mass nuclei [51], and others.

Note that the differences between the above-mentioned families of potentials are in the off-shell character, which is not an observable. Thus, any off-shell behavior of a NN potential is legitimate. There is no wrong off-shell character. However, some off-shell behaviors may lead in a more efficient way to realistic results than others. That is of interest to the many-body practitioner. We are now in a position to systematically investigate this issue for chiral forces.

Acknowledgments

The work by R.M. and Y.N. was supported in part by the U.S. Department of Energy under Grant No. DE-FG02-03ER41270. The work by D.R.E. has been partially funded by MINECO under Contracts No. FPA2013-47433-C2-2-P and FPA2016-77177-C2-2-P, and by the Junta de Castilla y Leon under Contract No. SA041U16.

Appendix A: Phaseshift tables

In this appendix, we show the phase shifts as predicted by the N⁴LO potential with $\Lambda = 500$ MeV. Note that our pp phase shifts are the phase shifts of the nuclear plus relativistic Coulomb interaction with respect to Coulomb

TABLE X: pp phase shifts (in degrees) up to F -waves at $N^4\text{LO}$ ($\Lambda = 500$ MeV).

T_{lab} (MeV)	1S_0	3P_0	3P_1	1D_2	3P_2	3F_2	ϵ_2	3F_3	3F_4
1	32.79	0.14	-0.08	0.00	0.01	0.00	0.00	0.00	0.00
5	54.84	1.61	-0.89	0.04	0.23	0.00	-0.05	0.00	0.00
10	55.20	3.79	-2.02	0.17	0.69	0.01	-0.20	-0.03	0.00
25	48.62	8.66	-4.84	0.69	2.57	0.11	-0.81	-0.23	0.02
50	38.84	11.42	-8.26	1.67	5.87	0.35	-1.69	-0.68	0.12
100	24.97	9.15	-13.48	3.61	10.70	0.83	-2.62	-1.46	0.51
150	15.04	4.55	-17.72	5.45	13.57	1.16	-2.83	-1.98	1.07
200	7.10	-0.47	-21.39	7.22	15.54	1.20	-2.71	-2.31	1.67
250	0.11	-5.89	-25.12	8.85	17.01	0.92	-2.42	-2.48	2.20
300	-6.43	-11.40	-29.35	9.91	17.84	0.35	-1.99	-2.46	2.59

TABLE XI: nn phase shifts (in degrees) up to F -waves at $N^4\text{LO}$ ($\Lambda = 500$ MeV).

T_{lab} (MeV)	1S_0	3P_0	3P_1	1D_2	3P_2	3F_2	ϵ_2	3F_3	3F_4
1	57.62	0.21	-0.12	0.00	0.02	0.00	0.00	0.00	0.00
5	61.01	1.88	-1.03	0.05	0.28	0.00	-0.06	-0.01	0.00
10	57.82	4.16	-2.21	0.18	0.78	0.01	-0.22	-0.04	0.00
25	49.11	9.01	-5.08	0.73	2.77	0.11	-0.84	-0.24	0.02
50	38.71	11.55	-8.52	1.72	6.15	0.36	-1.72	-0.70	0.13
100	24.65	9.06	-13.76	3.68	11.02	0.84	-2.62	-1.48	0.53
150	14.70	4.40	-17.98	5.52	13.92	1.16	-2.82	-2.00	1.09
200	6.74	-0.63	-21.62	7.28	15.94	1.20	-2.68	-2.32	1.70
250	-0.28	-6.02	-25.32	8.88	17.42	0.91	-2.36	-2.49	2.23
300	-6.87	-11.40	-29.48	9.87	18.24	0.32	-1.93	-2.46	2.61

wave functions. For nn and np scattering, our phase shifts are the ones from the nuclear interaction with respect to Riccati-Bessel functions. For more technical details of our phase shift calculations, we refer the interested reader to the appendix A3 of Ref. [65].

TABLE XII: $I = 1$ np phase shifts (in degrees) up to F -waves at $N^4\text{LO}$ ($\Lambda = 500$ MeV).

T_{lab} (MeV)	1S_0	3P_0	3P_1	1D_2	3P_2	3F_2	ϵ_2	3F_3	3F_4
1	62.00	0.18	-0.11	0.00	0.02	0.00	0.00	0.00	0.00
5	63.47	1.66	-0.92	0.04	0.27	0.00	-0.05	0.00	0.00
10	59.72	3.72	-2.03	0.16	0.75	0.01	-0.19	-0.03	0.00
25	50.48	8.25	-4.79	0.68	2.66	0.09	-0.76	-0.20	0.02
50	39.83	10.69	-8.20	1.68	5.96	0.31	-1.62	-0.61	0.11
100	25.68	8.25	-13.44	3.68	10.76	0.78	-2.53	-1.35	0.49
150	15.78	3.63	-17.67	5.56	13.63	1.08	-2.76	-1.86	1.04
200	7.90	-1.37	-21.33	7.34	15.63	1.12	-2.64	-2.18	1.64
250	0.96	-6.75	-25.05	8.96	17.12	0.83	-2.35	-2.35	2.17
300	-5.57	-12.14	-29.23	9.96	17.95	0.25	-1.93	-2.34	2.55

TABLE XIII: $I = 0$ np phase shifts (in degrees) at N⁴LO ($\Lambda = 500$ MeV).

T_{lab} (MeV)	1P_1	3S_1	3D_1	ϵ_1	3D_2	1F_3	3D_3	3G_3	ϵ_3
1	-0.19	147.75	-0.01	0.11	0.01	0.00	0.00	0.00	0.00
5	-1.50	118.17	-0.19	0.68	0.22	-0.01	0.00	0.00	0.01
10	-3.06	102.61	-0.69	1.17	0.85	-0.07	0.00	0.00	0.08
25	-6.32	80.66	-2.83	1.79	3.71	-0.42	0.02	-0.05	0.56
50	-9.66	62.91	-6.48	2.03	8.82	-1.13	0.20	-0.26	1.62
100	-14.78	43.72	-12.20	2.09	16.51	-2.19	1.10	-0.94	3.54
150	-19.52	31.42	-16.34	2.33	21.08	-2.92	2.29	-1.76	4.95
200	-23.46	21.60	-19.55	2.99	23.89	-3.54	3.40	-2.57	5.90
250	-25.72	12.68	-22.01	4.09	25.21	-4.14	4.23	-3.24	6.40
300	-25.27	4.02	-23.38	5.34	24.41	-4.69	4.78	-3.65	6.39

- [1] R. Machleidt and D. R. Entem, Phys. Rep. **503**, 1 (2011).
- [2] E. Epelbaum, H.-W. Hammer, and U.-G. Meißner, Rev. Mod. Phys. **81**, 1773 (2009).
- [3] J. Gasser and H. Leutwyler, Ann. Phys. (N.Y.) **158**, 142 (1984).
- [4] J. Gasser, M. E. Sainio, and A. Švarc, Nucl. Phys. **B307**, 779 (1988).
- [5] S. Weinberg, Phys. Lett **B251**, 288 (1990); Nucl. Phys. **B363**, 3 (1991).
- [6] C. Ordóñez, L. Ray, and U. van Kolck, Phys. Rev. Lett. **72**, 1982 (1994); Phys. Rev. C **53**, 2086 (1996).
- [7] N. Kaiser, R. Brockmann, and W. Weise, Nucl. Phys. **A625**, 758 (1997).
- [8] N. Kaiser, S. Gerstendörfer, and W. Weise, Nucl. Phys. **A637**, 395 (1998).
- [9] N. Kaiser, Phys. Rev. C **61**, 014003 (2000).
- [10] N. Kaiser, Phys. Rev. C **62**, 024001 (2000).
- [11] N. Kaiser, Phys. Rev. C **63**, 044010 (2001).
- [12] N. Kaiser, Phys. Rev. C **64**, 057001 (2001).
- [13] N. Kaiser, Phys. Rev. C **65**, 017001 (2002).
- [14] E. Epelbaum, W. Glöckle, and U.-G. Meißner, Nucl. Phys. **A637**, 107 (1998); **A671**, 295 (2000).
- [15] D. R. Entem and R. Machleidt, Phys. Rev. C **66**, 014002 (2002).
- [16] D. R. Entem and R. Machleidt, Phys. Rev. C **68**, 041001 (2003).
- [17] E. Epelbaum, W. Glöckle, and U.-G. Meißner, Nucl. Phys. **A747**, 362 (2005).
- [18] P. Navrátil, Few Body Syst. **41**, 117 (2007).
- [19] A. Ekström *et al.*, Phys. Rev. Lett. **110**, 192502 (2013).
- [20] A. Gezerlis, I. Tews, E. Epelbaum, M. Freunek, S. Gandolfi, K. Hebeler, A. Nogga, and A. Schwenk, Phys. Rev. C **90**, 054323 (2014).
- [21] M. Piarulli, L. Girlanda, R. Schiavilla, R. Navarro Pérez, J. E. Amaro, and E. Ruiz Arriola, Phys. Rev. C **91**, 024003 (2015).
- [22] M. Piarulli, L. Girlanda, R. Schiavilla, A. Kievsky, A. Lovato, L. E. Marcucci, Steven C. Pieper, M. Viviani, and R. B. Wiringa, Phys. Rev. C **94**, 054007 (2016).
- [23] E. Epelbaum, H. Krebs, and Ulf-G. Meißner, Eur. Phys. J. A **51**, 53 (2015).
- [24] E. Epelbaum, H. Krebs, and Ulf-G. Meißner, Phys. Rev. Lett. **115**, 122301 (2015).
- [25] R. Navarro Pérez, J. E. Amaro, and E. Ruiz Arriola, Phys. Rev. C **91**, 054002 (2015), and more references to the *comprehensive* work by the Granada group therein.
- [26] A. Ekström *et al.*, Phys. Rev. C **91**, 051301 (2015).
- [27] B. D. Carlsson *et al.*, Phys. Rev. X **6**, 011019 (2016).
- [28] I. Tews, S. Gandolfi, A. Gezerlis, and A. Schwenk, Phys. Rev. C **93**, 024305 (2016).
- [29] J. E. Lynn, I. Tews, J. Carlson, S. Gandolfi, A. Gezerlis, K. E. Schmidt, and A. Schwenk, Phys. Rev. Lett. **116**, 062501 (2016).
- [30] Xiu-Lei Ren, Kai-Wen Li, Li-Sheng Geng, Bingwei Long, Peter Ring, and Jie Meng, Leading order covariant chiral nucleon-nucleon interaction, arXiv:1611.08475 [nucl-th].
- [31] E. Epelbaum, A. Nogga, W. Gloeckle, H. Kamada, U. G. Meissner, and H. Witala, Phys. Rev. C **66**, 064001 (2002).
- [32] P. Navrátil, R. Roth, and S. Quaglioni, Phys. Rev. C **82**, 034609 (2010).
- [33] M. Viviani, L. Girlanda, A. Kievsky, and L. E. Marcucci, Phys. Rev. Lett. **111**, 172302 (2013).
- [34] J. Golak *et al.*, Eur. Phys. J. A **50**, 177 (2014).
- [35] B. R. Barrett, P. Navrátil, and J. P. Vary, Prog. Part. Nucl. Phys. **69**, 131 (2013).
- [36] H. Hergert, S. K. Bogner, S. Binder, A. Calci, J. Langhammer, R. Roth, and A. Schwenk, Phys. Rev. C **87**, 034307

- (2013).
- [37] G. Hagen, T. Papenbrock, M. Hjorth-Jensen, and D. J. Dean, Rept. Prog. Phys. **77**, 096302 (2014).
 - [38] J. Simonis, S. R. Stroberg, K. Hebeler, J. D. Holt, and A. Schwenk, “Saturation with chiral interactions and consequences for finite nuclei,” arXiv:1704.02915 [nucl-th].
 - [39] K. Hebeler and A. Schwenk, Phys. Rev. C **82**, 014314 (2010).
 - [40] K. Hebeler, S. K. Bogner, R. J. Furnstahl, A. Nogga, and A. Schwenk, Phys. Rev. C **83**, 031301(R) (2011).
 - [41] G. Hagen, T. Papenbrock, A. Ekström, K. A. Wendt, G. Baardsen, S. Gandolfi, M. Hjorth-Jensen, and C. J. Horowitz, Phys. Rev. C **89**, 014319 (2014).
 - [42] L. Coraggio, J. W. Holt, N. Itaco, R. Machleidt, and F. Sammarruca, Phys. Rev. C **87**, 014322 (2013).
 - [43] L. Coraggio, J. W. Holt, N. Itaco, R. Machleidt, L. E. Marcucci, and F. Sammarruca, Phys. Rev. C **89**, 044321 (2014).
 - [44] F. Sammarruca, L. Coraggio, J. W. Holt, N. Itaco, R. Machleidt, and L. E. Marcucci, Phys. Rev. C **91**, 054311 (2015).
 - [45] D. R. Entem, R. Machleidt, and H. Witala, Phys. Rev. C **65**, 064005 (2002).
 - [46] H. Krebs, A. Gasparyan, and E. Epelbaum, Phys. Rev. C **85**, 054006 (2012).
 - [47] H. Krebs, A. Gasparyan, and E. Epelbaum, Phys. Rev. C **87**, 054007 (2013).
 - [48] E. Epelbaum, A. M. Gasparyan, H. Krebs, and C. Schat, Eur. Phys. J. A **51**, 26 (2015).
 - [49] L. Girlanda, A. Kievsky, M. Viviani, Phys. Rev. C **84**, 014001 (2011).
 - [50] V. Lapoux, V. Somà, C. Barbieri, H. Hergert, J. D. Holt, and S. R. Stroberg, Phys. Rev. Lett. **117**, 052501 (2016).
 - [51] S. Binder, J. Langhammer, A. Calci, and R. Roth, Phys. Lett. B **736**, 119 (2014).
 - [52] D. R. Entem, N. Kaiser, R. Machleidt, and Y. Nosyk, Phys. Rev. C **91**, 014002 (2015).
 - [53] D. R. Entem, N. Kaiser, R. Machleidt, and Y. Nosyk, Phys. Rev. C **92**, 064001 (2015).
 - [54] R. J. Furnstahl, D. R. Phillips, and S. Wesolowski, J. Phys. G **42**, 034028 (2015).
 - [55] J. A. Melendez, S. Wesolowski, and R. J. Furnstahl, Bayesian truncation errors in chiral effective field theory: nucleon-nucleon observables, arXiv:1704.03308 [nucl-th], and references therein.
 - [56] K. A. Olive *et al.* (Particle Data Group), Chin. Phys. C **38**, 090001 (2014).
 - [57] G. Q. Li and R. Machleidt, Phys. Rev. C **58**, 3153 (1998).
 - [58] E. Epelbaum, W. Glöckle, and U.-G. Meißner, Eur. Phys. J. A **19**, 125 (2004).
 - [59] 2015 Dr. Klaus Erkelenz Price Winners, University of Bonn, Germany; for more information, see <https://www.hiskp.uni-bonn.de>
 - [60] M. Hoferichter, J. Ruiz de Elvira, B. Kubis, and U.-G. Meißner, Phys. Rev. Lett. **115**, 192301 (2015); Phys. Rep. **625**, 1 (2016).
 - [61] G. J. M. Austin and J. J. de Swart, Phys. Rev. Lett. **50**, 2039 (1983).
 - [62] J. R. Bergervoet, P. C. van Campen, W. A. van der Sanden, and J. J. de Swart, Phys. Rev. C **38**, 15 (1988).
 - [63] U. van Kolck, M. C. M. Rentmeester, J. L. Friar, T. Goldman, and J. J. de Swart, Phys. Rev. Lett. **80**, 4386 (1998).
 - [64] R. Blankenbecler and R. Sugar, Phys. Rev. **142**, 1051 (1966).
 - [65] R. Machleidt, Phys. Rev. C **63**, 024001 (2001).
 - [66] K. Erkelenz, R. Alzetta, and K. Holinde, Nucl. Phys. **A176**, 413 (1971).
 - [67] R. Machleidt, in: *Computational Nuclear Physics 2 – Nuclear Reactions*, edited by K. Langanke, J.A. Maruhn, and S.E. Koonin (Springer, New York, 1993) p. 1.
 - [68] D. B. Kaplan, M. Savage, and M. B. Wise, Nucl. Phys. **B478**, 629 (1996); Phys. Lett. *B424*, 390 (1998); Nucl. Phys. **B534**, 329 (1998).
 - [69] M. C. Birse, Phys. Rev. C **74**, 014003 (2006); *ibid.* **76**, 034002 (2007); *ibid.* **77**, 047001 (2008).
 - [70] B. Long and C. Yang, Phys. Rev. C **86**, 024001 (2012).
 - [71] B. Long, Int. J. Mod. Phys. E **25**, 1641006 (2016).
 - [72] M. P. Valderrama, Int. J. Mod. Phys. E **25**, 1641007 (2016).
 - [73] M. P. Valderrama, M. Sanchez Sanchez, C.-J. Yang, Bingwei Long, J. Carbonell, and U. van Kolck, Power Counting in Peripheral PartialWaves: The Singlet Channels, arXiv:1611.10175.
 - [74] M. Sanchez Sanchez, C.-J. Yang, Bingwei Long, and U. van Kolck, The Two-Nucleon 1S_0 Amplitude Zero in Chiral Effective Field Theory, arXiv:1704.08524.
 - [75] E. Epelbaum, J. Gegelia, and Ulf-G. Meißner, Wilsonian renormalization group versus subtractive renormalization in effective field theories for nucleon-nucleon scattering, arXiv:1705.02524.
 - [76] S. König, H. W. Griesshammer, H.-W. Hammer, and U. van Kolck, Phys. Rev. Lett. **118**, 202501 (2017).
 - [77] G. P. Lepage, How to Renormalize the Schrödinger Equation, arXiv:nucl-th/9706029.
 - [78] E. Marji *et al.*, Phys. Rev. C **88**, 054002 (2013).
 - [79] J. R. Bergervoet, P. C. van Campen, R. A. M. Klomp, J.-L. de Kok, T. A. Rijken, V. G. J. Stoks, and J. J. de Swart, Phys. Rev. C **41**, 1435 (1990).
 - [80] V. G. J. Stoks, R. A. M. Klomp, M. C. M. Rentmeester, and J. J. de Swart, Phys. Rev. C **48**, 792 (1993).
 - [81] F. Gross and A. Stadler, Phys. Rev. C **78**, 014005 (2008).
 - [82] R. Navarro Pérez, J. E. Amaro, and E. Ruiz Arriola, Phys. Rev. C **88**, 064002 (2013).
 - [83] D. Albers *et al.*, Eur. Phys. J. A **22**, 125 (2004).
 - [84] N. Hoshizaki, Prog. Theor. Phys. Suppl. **42**, 107 (1968).
 - [85] J. Bystricky, F. Lehar, and P. Winterschnitz, J. Phys. (Paris) **39**, 1 (1978).
 - [86] W. P. Abfalterer, F. B. Bateman, F. S. Dietrich, R. W. Finlay, R. C. Haight, and G. L. Morgan, Phys. Rev. C **63**, 044608 (2001).
 - [87] N. Boukharouba, F. B. Bateman, C. E. Brient, A. D. Carlson, S. M. Grimes, R. C. Haight, T. N. Massey, and O. A.

- Wasson, Phys. Rev. C **65**, 014004 (2002).
- [88] P. Mermod *et al.*, Phys. Lett. B **597**, 243 (2004).
- [89] P. Mermod *et al.*, Phys. Rev. C **72**, 061002 (2005).
- [90] J. Klug *et al.*, Nucl. Instrum. Methods A **489**, 282 (2002).
- [91] V. Blideanu *et al.*, Phys. Rev. C **70**, 014607 (2004).
- [92] C. Johansson *et al.*, Phys. Rev. C **71**, 024002 (2005).
- [93] J. Arnold *et al.*, Eur. Phys. J. C **17**, 67 (2000).
- [94] J. Arnold *et al.*, Eur. Phys. J. C **17**, 83 (2000).
- [95] M. Daum *et al.*, Eur. Phys. J. C **25**, 55 (2002).
- [96] V. Stoks and J. J. de Swart, Phys. Rev. C **47**, 761 (1993).
- [97] V. G. J. Stoks, R. A. M. Klomp, C. P. F. Terheggen, and J. J. de Swart, Phys. Rev. C **49**, 2950 (1994).
- [98] R. B. Wiringa, V. G. J. Stoks, and R. Schiavilla, Phys. Rev. C **51**, 38 (1995).
- [99] R. Machleidt, K. Holinde, and Ch. Elster, Phys. Rep. **149**, 1 (1987).
- [100] R. A. Arndt, W. J. Briscoe, I. I. Strakovsky, and R. L. Workman, Phys. Rev. C **76**, 025209 (2007).
- [101] V. G. J. Stoks (private communication).
- [102] W. A. van der Sanden, A. H. Emmen, and J. J. de Swart, Report No. THEF-NYM-83.11, Nijmegen (1983), unpublished; quoted in Ref. [62].
- [103] D. E. González Trotter *et al.*, Phys. Rev. C **73**, 034001 (2006).
- [104] Q. Chen *et al.*, Phys. Rev. C **77**, 054002 (2008).
- [105] G. A. Miller, M. K. Nefkens, and I. Slaus, Phys. Rep. **194**, 1 (1990).
- [106] U. D. Jentschura, A. Matveev, C. G. Parthey, J. Alnis, R. Pohl, Th. Udem, N. Kolachevsky, and T. W. Hänsch, Phys. Rev. A **83**, 042505 (2011).
- [107] W. N. Polyzou and W. Glöckle, Few-Body Syst. **9**, 97 (1990).
- [108] U. van Kolck, Phys. Rev. C **49**, 2932 (1994).
- [109] V. Bernard, E. Epelbaum, H. Krebs, and Ulf-G. Meißner, Phys. Rev. C **77**, 064004 (2008).
- [110] V. Bernard, E. Epelbaum, H. Krebs, and Ulf-G. Meißner, Phys. Rev. C **84**, 054001 (2011).
- [111] K. Hebeler, H. Krebs, E. Epelbaum, J. Golak, and R. Skibinski, Phys. Rev. C **91**, 044001 (2015).
- [112] R. A. Arndt, W. J. Briscoe, I. I. Strakovsky, and R. L. Workman, Phys. Rev. C **74**, 045205 (2006).
- [113] J.-I. Fujita and H. Miyazawa, Prog. Theor. Phys. **17**, 360 (1957).
- [114] R. Navarro Perez, J. E. Amaro, and E. Ruiz Arriola, Phys. Rev. C **89**, 064006 (2014).
- [115] R. Navarro Perez, E. Garrido, J. E. Amaro, and E. Ruiz Arriola, Phys. Rev. C **90**, 047001 (2014).
- [116] R. Navarro Perez, J. E. Amaro, E. Ruiz Arriola, P. Maris, and J. P. Vary, Phys. Rev. C **92**, 064003 (2015).
- [117] A. Nogga, P. Navratil, B. R. Barrett, and J. P. Vary, Phys. Rev. C **73** (2006) 064002.
- [118] A. Gärdestig and D. R. Philips, Phys. Rev. Lett. **96** (2006) 232301.
- [119] D. Gazit, S. Quaglioni, and P. Navrátil, Phys. Rev. Lett. **103** (2009) 102502.
- [120] L. E. Marcucci, A. Kievsky, S. Rosati, R. Schiavilla, and M. Viviani, Phys. Rev. Lett. **108**, 052502 (2012).
- [121] P. Navratil, V. G. Gueorguiev, J. P. Vary, W. E. Ormand, and A. Nogga, Phys. Rev. Lett. **99** (2007) 042501.
- [122] T. Krüger, I. Tews, K. Hebeler, and A. Schwenk, Phys. Rev. C **88**, 025802 (2013).
- [123] C. Drischler, K. Hebeler, and A. Schwenk, Phys. Rev. C **93**, 054314 (2016).
- [124] C. Drischler, A. Carbone, K. Hebeler, and A. Schwenk, Phys. Rev. C **94**, 054307 (2016).
- [125] User-friendly FORTRAN codes for all NN potentials presented in this paper can be obtained from the authors upon request.

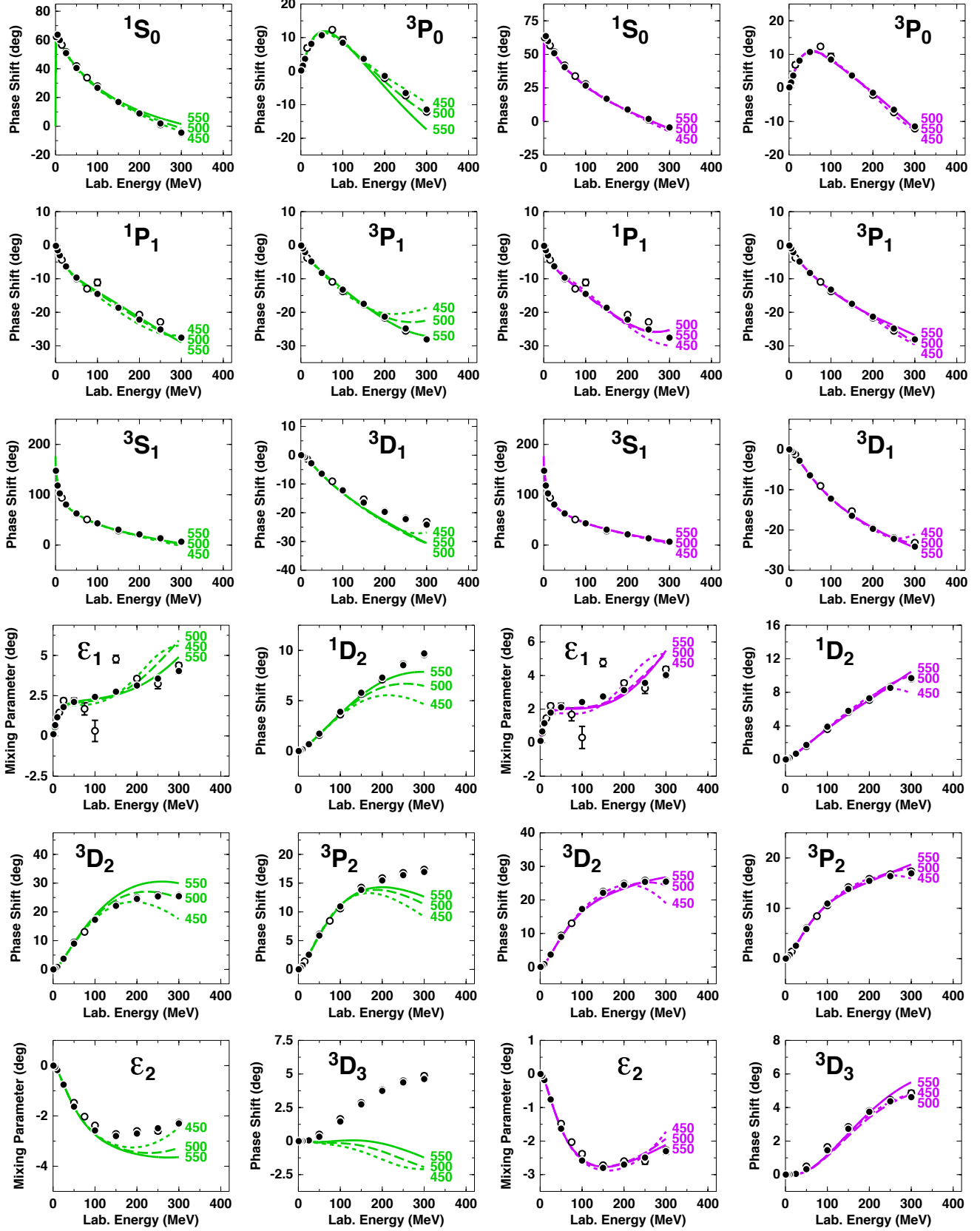


FIG. 3: (Color online). Cutoff variations of the np phase shifts at NNLO (left side, green lines) and N^4 LO (right side, purple lines). Dotted, dashed, and solid lines represent the results obtained with cutoff parameter $\Lambda = 450, 500,$ and 550 MeV, respectively, as also indicated by the curve labels. Note that, at N^4 LO, the cases 500 and 550 MeV cannot be distinguished on the scale of the figures for most partial waves. Filled and open circles as in Fig. 2.